UNIVERSITY OF BIRMINGHAM

STUDIES ON THE ROLE OF CLEC-2 AND SYK IN LYMPHATIC DEVELOPMENT AND RESPONSE TO RADIATION

A ROLE FOR ATRIAL NATIURETIC PEPTIDE IN PLATELET INHIBITION AND EVIDENCE FOR COMPARTMENTATION OF cGMP SIGNALLING

KATE LOWE

August 2011

Centre for Cardiovascular Sciences

Institute of Biomedical Research

College of Medical and Dental Services

University of Birmingham

UNIVERSITY OF
BIRMINGHAM

University of Birmingham Research Archive

e-theses repository

This unpublished thesis/dissertation is copyright of the author and/or third parties. The intellectual property rights of the author or third parties in respect of this work are as defined by The Copyright Designs and Patents Act 1988 or as modified by any successor legislation.

Any use made of information contained in this thesis/dissertation must be in accordance with that legislation and must be properly acknowledged. Further distribution or reproduction in any format is prohibited without the permission of the copyright holder.

STUDIES ON THE ROLE OF CLEC-2 AND SYK IN LYMPHATIC DEVELOPMENT AND RESPONSE TO RADIATION

KATE LOWE

A thesis submitted to the University of Birmingham in part requirement for the award of MRes

Centre for Cardiovascular Sciences

Institute of Biomedical Research

College of Medical and Dental Services

University of Birmingham

August 2011

Abstract

The platelet C type lectin-like type II (CLEC-2) transmembrane receptor has been shown to interact with its endogenous ligand, podoplanin, on lymphatic endothelium and mediate separation from blood vessels. Here, conditional deletion of CLEC-2 or a mutation in signalling molecule Syk, specifically in the megakaryocyte/platelet lineage, was seen to cause a severe blood-lymphatic mixing phenotype. As constitutive loss of CLEC-2 in mice is lethal at birth, radiation chimeras have been pivotal to investigating the role of CLEC-2 in platelet function. This pilot study was conducted to investigate the role of platelets in the recovery from radiation injury. Mice were subjected to irradiation and reconstituted with *CLEC-2*$^{+/+}$ or *CLEC-2*$^{-/-}$ foetal liver cells. Immunofluorescence in the intestinal mesentery at 9 days showed disrupted vasculature in *CLEC-2*$^{-/-}$ mice. The only visible difference between the two sets of chimeras was blood in the intestine of *CLEC-2*$^{-/-}$ mice at 28 days. Terminal deoxynucleotidyl end labeling (TUNEL) showed no difference in the percentage of apoptotic cells in the livers of *CLEC-2*$^{+/+}$ and *CLEC-2*$^{-/-}$ mice but an increase in the spleen. These results support the idea of a progressive intestinal phenotype and support a role for CLEC-2 and Syk in the separation and organization of blood and lymphatic vessels.

Acknowledgements

Special thanks to Professor Steve Watson and Dr Brenda Finney for supervising this project, to all members of the Watson group for their help and support and to the Medical Research Council for funding this work.

Contents

1.0. Introduction 1

1.1. Platelet function and signalling 1

1.2. CLEC-2 2

1.3. Development of blood and lymphatic vasculature 4

1.4. The role of platelets and CLEC-2 in lymphatic development 5

1.5. Radiation chimeras in investigating damage and recovery processes 6

1.6. Aims of the study 7

2.0 Methods 8

2.1. Materials 8

2.2. Genotyping 9

2.3. Animal studies 10

2.31. Radiation chimera studies 10

2.32. Harvesting and fixing CLEC-2 and R41A embryos 12

2.4. Immunofluorescence staining 12

2.41. Whole mount 12

2.42. Immunofluorescence of cryosections 13

2.43. Immunohistochemistry 14

2.44. TUNEL assay 15

3.0. Results 16

3.1. Genotyping and phenotyping R41A mice 16

3.2. Optimising protocols for immunostaining 17

3.21. Immunohistochemistry of paraffin sections 17

3.22. Immunofluorescence of frozen sections 18

3.3. Investigating damage and recovery processes in radiation chimeras 19

3.31. Platelet studies 19

3.32. Phenotyping radiation chimeras 20

3.33. TUNEL labelling of apoptotic cells 21

4.0 Discussion 23

4.1. *R41A*$^{fl/fl}$*PF4-Cre* embryos phenocopy *CLEC-2*$^{fl/fl}$*PF4-Cre* embryos 23

4.2. Obstacles faced in optimising immunofluorescence of frozen sections 25

4.3. Investigating damage and recovery processes in radiation chimeras 27

4.31. No difference observed in platelet count recovery between *CLEC-2*$^{-/-}$ and *CLEC-2*$^{+/+}$ chimeras 27

4.32. *CLEC-2*$^{-/-}$ chimeras show signs of a progressive intestinal phenotype 28

4.33. Radiation induces elevated levels of apoptosis in liver and spleen 30

5.0. Conclusion 32

6.0. Future directions 33

7.0. Figures 35

List of Figures and Tables

Figure 1. Recruitment of Syk to platelet signalling molecules, GPVI, CLEC-2 and integrin αIIbβ3. 3

Figure 2. Genetic strategy and genotyping of R41A mice. 36

Figure 3. Phenotyping *R41A*$^{fl/fl}$PF4-Cre and *Clec-2*$^{fl/f}$*PF4-Cre* embryos at E14.5.... 37

Figure 4. Immunostaining for podoplanin in adult lung paraffin sections. 38

Figure 5. Prox-1 immunostaining of LEC's in *CLEC-2*$^{+/+}$ lung paraffin sections at E16.5. 39

Figure 6. Immunofluorescence of mouse adult lung sections with pro-SP-C. 40

Figure 7. Immunofluorescence of frozen sections with CD31-FITC..... 41

Figure 8. Generation and analysis of radiation chimeras. 42

Figure 9. Analysis of platelets in whole blood of radiation chimeras. 43

Figure 10. FACS analysis of PRP at days 21 and 28 post radiation and reconstitution. 44

Figure 11. Analysis of the intestinal phenotype in radiation chimeras. 45

Figure 12. Whole mount immunofluorescence staining of the intestinal mesentery. 46

Figure 13. Schematic diagram of the TUNEL assay technique for detection of apoptotic cells..... 47

Figure 14. Visualising rhodamine labelled apoptotic cells. 48

Figure 15. Quantifying the level of apoptosis occurring in spleen and liver sections of radiation chimeras. 49

Table 1. Primer sequences for *CLEC-2*$^{+/+}$, *CLEC-2*$^{-/-}$, R41A and PF4-Cre genotyping..... 50

List of Abbreviations

CLEC-2, C-type lectin-like type II receptor; E, embryonic day; FACS, fluorescence activated cell sorting; Fcr, Fc receptor; IHC, immunohistochemistry; ITAM, immunoreceptor tyrosine-based activation motif; LEC, lymphatic endothelial cell; Lyve-1, lymphatic vessel endothelial hyaluronan receptor-1; MPV, mean platelet volume; PF4, platelet factor 4; PRP, platelet rich plasma; Prox-1, prospero-related homeobox-1; SFK, Src family kinase; TUNEL, terminal deoxynucleotidyl transferase (TdT) dUTP nick end labelling.

1.0. Introduction

1.1. Platelet function and signalling

Platelet activation and the formation of platelet aggregates play vital physiological roles in maintaining vascular integrity and preventing severe blood loss resulting from tissue trauma. However, platelets can also respond to atherosclerotic plaque rupture leading to myocardial infarction or stroke[1]. The main platelet activating glycoproteins and their intricate signalling pathways have thus become key therapeutic targets. Platelet activation in response to soluble platelet ligands such as thrombin, ADP or thromboxane A2 occurs through heterotrimeric G proteins which orchestrate the activation of several downstream effectors[2]. The major platelet collagen receptor, GPVI, activates platelets through an alternative mechanism, involving a sequential multi-step pathway in which Src family kinases (SFK) phosphorylate the immunoreceptor tyrosine-based activation motif (ITAM) in the Fc receptor (Fcr) γ-chain to which the tyrosine kinase Syk is recruited[3]. A similar mechanism is employed by CLEC-2, however, here SFK's are thought to modulate Syk activity which directly mediates phosphorylation of the tyrosine residues in the CLEC-2 cytoplasmic tail and hence its own recruitment[4]. In contrast, Syk is recruited independently of an ITAM to the platelet integrin αIIbβ3, associating with the integrin β3 cytoplasmic tail (Figure 1). Despite these differences, each pathway uses a similar, yet distinct series of downstream signalling proteins to ultimately activate PLCγ2 and induce various platelet activating effects[5].

1.2. CLEC-2

CLEC-2 is a 30 kDa type II transmembrane protein expressed at high levels on platelets and megakaryocytes with low expression on a subpopulation of other hematopoietic cells. Initial identification and characterisation of CLEC-2 was achieved through the observed potent platelet activation induced by the exogenous ligand, the snake venom toxin, rhodocytin[6]. Following this, the transmembrane glycoprotein podoplanin was discovered as an endogenous ligand for CLEC-2, eliciting powerful platelet activation and secretion in a manner reminiscent to rhodocytin. Podoplanin is expressed on type 1 lung alveolar cells, lymphatic endothelium, kidney podocytes and tumour cells and remains the only known endogenous ligand for CLEC-2 to date[7]. CLEC-2 appears to play a fundamental role in thrombus formation, however, given the absence of a ligand for CLEC-2 in the blood vasculature, the mechanism behind its role in hemostasis and thrombosis remains unknown[8-10].

As discussed, platelet receptors GPVI and CLEC-2 utilise a similar niche of downstream signalling proteins but the initial recruitment of tyrosine kinase Syk occurs via two distinct mechanisms. The GPVI receptor recruits Syk via its tandem SH2 domains to the phosphorylated tyrosine residues within its two YxxL motifs (ITAMs) in the Fc γ-chain (Figure 1)[2]. In contrast, CLEC-2 has only a single YxxL motif in its cytoplasmic tail, known as a hemiITAM, and it is suggested that CLEC-2 signals through a unique crosslinking mechanism encompassing two phosphorylated hemi-ITAMs, bridged by a single Syk molecule (Figure 1)[4, 11].

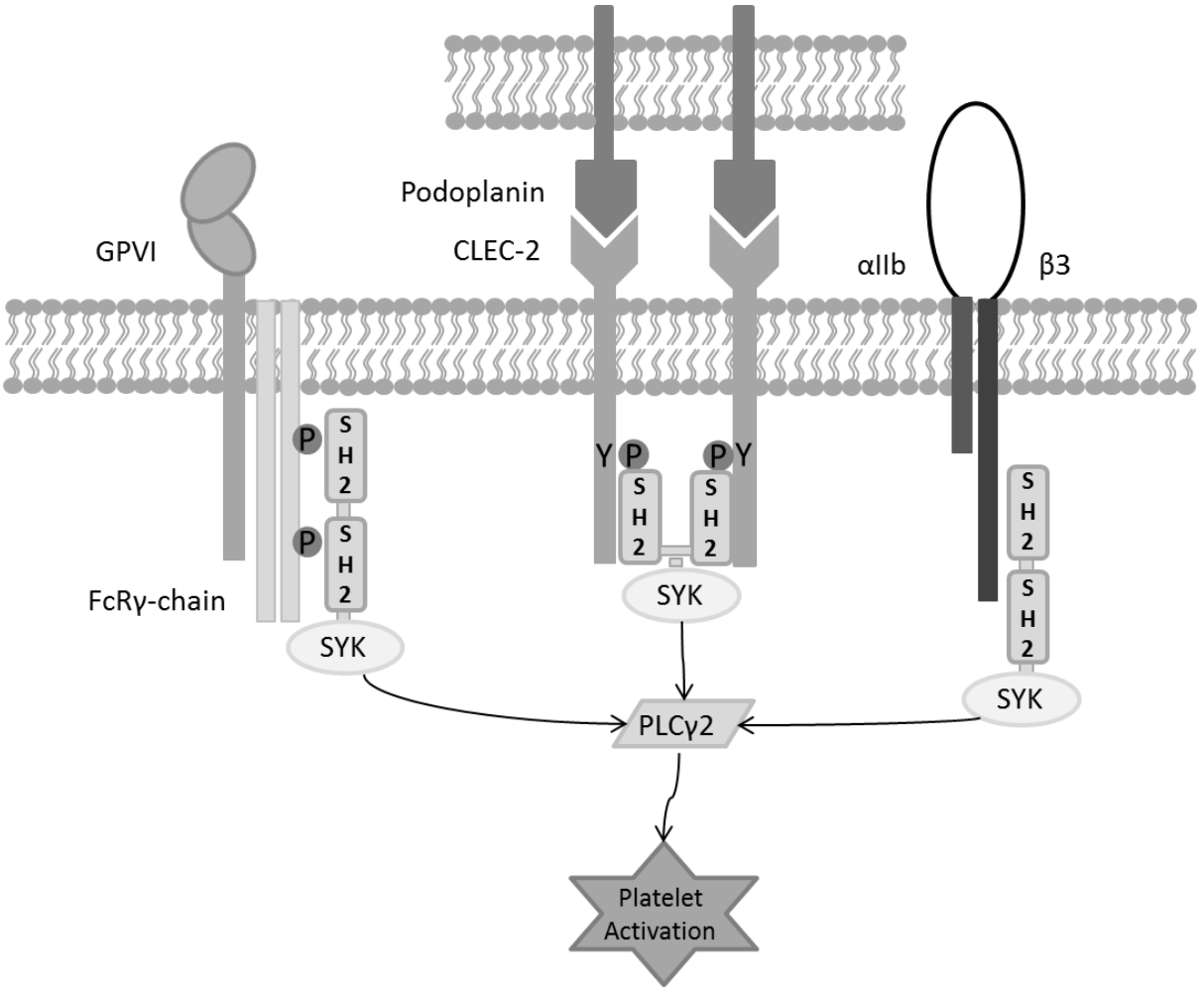

Figure 1. *Recruitment of Syk to platelet signalling molecules, GPVI, CLEC-2 and integrin αIIbβ3.* Tyrosine residues within the Fcr γ-chain of GPVI and the cytoplasmic tail of CLEC-2 become phosphorylated and recruit Syk through alternative mechanisms; Two ITAMs in the Fcr γ-chain bind a single Syk molecule whereas Syk crosslinks CLEC-2 through binding to a hemiITAM in each cytoplasmic tail. Conversely, the β3 tail of integrin αIIbβ3 interacts with the N-terminal SH2 domain of Syk independent of an ITAM. Each signalling pathway utilises varied downstream signalling molecules to ultimately activate PLC γ2. Modified from Watson et al 2005; 2010[2, 5].

1.3. Development of blood and lymphatic vasculature

The lymphatic system consists of a vast capillary network that functions to drain protein-rich interstitial fluid (lymph) from the extracellular spaces within organs and return it to the venous circulation. Other components of the lymphatic system include the lymphoid organs; spleen, Peyer's patches, lymph nodes, tonsils and thymus, which have essential roles in the immune response[12].

It is known that platelets appear in the circulation around embryonic day (E) 8.5, at which point the blood vasculature is already established. The lymphatic system develops secondary, yet parallel to the blood vasculature, appearing around E10.5, where according to Sabin's widely accepted model[13], endothelial cell budding from local veins migrate to form the primary lymph sacs. The lymphatic network then spreads through endothelial sprouting to peripheral organs and tissues to form local capillary networks[14].

Until recently, studying the process of lymphatic development has been hindered by the lack of lymphatic specific markers. The transmembrane glycoprotein, lymphatic vessel endothelial hyaluronan receptor 1 (Lyve-1), is expressed broadly throughout the embryonic vasculature and is thought to represent the earliest sign of lymphatic commitment[12, 15]. Subsequent loss of blood vascular markers and gain of the transcription factor, prospero related homeobox 1 (Prox-1), around E10.5, commits cells to bud from veins and differentiate into lymphatic endothelial cells (LECs)[16]. The mature lymphatic vasculature is completely independent of the blood vascular system aside from connections at the thoracic and right ducts with the subclavian vein, allowing the lymphatic drainage into the blood system

while preventing blood reflux into the lymphatic system through specialised valves[17].

1.4. The role of platelets and CLEC-2 in lymphatic development

A number of mouse models have been generated which show defects in the separation of blood vasculature from lymphatic vasculature resulting in the appearance of blood filled lymphatic vessels in the skin[17]. The mechanisms that mediate blood and lymphatic vascular separation during embryonic development are poorly understood. Podoplanin on the surface of LEC's has been found to interact with CLEC-2 on platelets to facilitate the separation of blood and lymphatic vessels[18]. Podoplanin deficient mice develop a severe blood-lymphatic mixing phenotype mid-gestation and die shortly after birth due to an inability to inflate their lungs[19, 20]. The appearance of blood-filled lymphatic vessels have also been seen in mice deficient in CLEC-2 or its downstream signalling partners, Syk, SLP-76 and PLC-γ2; notably, this defect does not manifest upon deletion of the GPVI FcR-γ chain or integrin αIIbβ3 which also signal through these proteins[9, 21-23]. Taken together, the discovery of podoplanin as an endogenous ligand for CLEC-2 suggests podoplanin on the surface of LEC's interacts with CLEC-2 on platelets to mediate the separation of blood and lymphatic vasculature, involving platelet signalling through Syk, SLP-76 and PLCγ2 (Finney et al, manuscript submitted for publication).

Recent work looking further into the role of CLEC-2 and Syk in embryonic development led to the analysis of mice constitutively deficient in CLEC-2 (*CLEC-*

2$^{-/-}$) and Syk (*Syk*$^{-/-}$) and compared these to mice containing a specific deletion of CLEC-2 or Syk in the megakaryocyte/platelet lineage. Both constitutive and platelet specific *CLEC-2*$^{-/-}$ and *Syk*$^{-/-}$ embryos presented with oedema, haemorrhaging in the brain and evidence of blood filled lymphatic vessels (Finney et al, manuscript in preparation).

In order to further dissect the specific platelet signalling pathways involved in the separation of blood and lymphatic vasculature, a second mouse model was generated containing a mutated arginine residue (R41A) in the SH2 domain of tyrosine kinase Syk. The R41A mutation specifically prevents Syk interacting with the phosphorylated hemiITAM and ITAM receptors, such as CLEC-2 and GPVI, leaving the Syk interaction with other platelet receptors, such as integrins, unperturbed.

1.5. Radiation chimeras in investigating damage and recovery processes

Constitutive *CLEC-2*$^{-/-}$ mice are embryonically lethal. Bone marrow radiation chimeras provide a means for producing adult mice with platelets lacking CLEC-2[10]. In this model, irradiation kills all rapidly proliferating and haematopoietic progenitor cells, including those of the platelet lineage and allows effective reconstitution of the bone marrow with a donor foetal liver cell line carrying the mutation of interest[24]. Irradiation suppresses the host immune system to allow the graft time to manifest immunological competence; however, in extreme cases the host may mount an overwhelming immune response against the graft resulting in rejection and possibly death. More generally, radiation chimeras manifest with

tissue damage, specifically to the lymphatic tissues (e.g. spleen and lymph nodes), gastrointestinal tract and the liver, although they recover[25].

Previous work in characterising CLEC-2 confirmed the successful application of irradiation in providing a selective loss of CLEC-2 in mice reconstituted with *CLEC-2*$^{-/-}$ foetal liver cells[10]. In addition, on-going work looking into the impaired recovery of lymphatic vessels when reconstituted with *CLEC-2*$^{-/-}$ as oppose to *CLEC-2*$^{+/+}$ foetal liver cells (Barone et at, unpublished observations), prompted the need for a pilot study to investigate the basal level of damage incurred by radiation and allow direct association of the effects caused by *CLEC-2*$^{-/-}$ platelets.

1.6. Aims of the study

The initial aim of the study was to genotype the R41A mice to confirm the presence of the megakaryocyte specific R41A Syk mutation. Through the use of timed matings, embryo dissection and photography, the phenotype of R41A embryos during development was to be recorded and comparisons made to the existing *CLEC-2*$^{-/-}$ phenotype.

To investigate the role of CLEC-2 and Syk in recovery to radiation damage, mice were to be subject to radiation and reconstitution with *CLEC-2*$^{+/+}$ or *CLEC-2*$^{-/-}$ foetal liver cells and sacrificed at different time points. Mice were phenotypically analysed, blood taken for platelet studies and tissues dissected for immunohistochemistry, immunofluorescence and TUNEL labelling to investigate the damage and recovery processes occurring.

2.0. Methods

2.1. Materials

Primary antibodies used in this study were rabbit anti-mouse Prox-1 (Abcam), rabbit anti-mouse Prox-1 (Angiobio), hamster anti-mouse podoplanin (Angiobio), rat anti-mouse EphrinB4 (Abcam), rabbit anti-mouse SP-C (Seven Hills), rat anti-mouse Endomucin (Santa Cruz Biotechnology), rat anti-mouse CD-31-FITC (BD biosciences), rabbit anti-mouse Lyve-1 (Abcam), rat anti-mouse CD41-FITC (BD Biosciences Pharmigen) and rat anti-mouse CLEC-2 was a gift from Caetano Reis e Sousa & Diego Mourão-Sá, Cancer research UK, London. Antibodies used for secondary detection were biotinylated goat anit-hamster IgG (Angiobio), FITC conjugated swine anti-rabbit IgG (Dako Cytomation), Alexa Fluor® 488- or 594 conjugated goat anti-rat IgG (Invitrogen), Alexa Fluor® 532 conjugated goat anti-rabbit IgG (Invitrogen). Additional materials used include optimum cutting temperature (O.C.T) compound (Cell Path), Dullbeccos 1 X PBS (Gibco), VECTASTAIN® Elite® ABC Reagent, DAB substrate chromagen and Vectormount mounting medium (Vector laboratories inc), *CLEC-2*$^{+/+}$, *CLEC-2*$^{-/-}$ and common primers (Invitrogen), R41A forward and reverse primers (Ozgene), R41 platelet factor 4 (PF4) Cre forward and reverse primers (Invitrogen). RedTaq®ReadyMix™ and Water PCR Reagent (Sigma Aldrich).

2.2. Genotyping

Mouse ear or tail clippings were digested in lysis buffer (100 mM Tris-HCL, 5 mM EDTA, 0.2% SDS, 200 mM NaCl, pH to 8.5) and proteinase K (1 µg/ml) overnight at 55°C. Samples were centrifuged at 13,000 g for 10 min to pellet undigested debris, isopropanol was added to supernatant and shaken until a DNA aggregate was visible which was transferred to approximately 80 µl of Millipore water, volume adjusted according to aggregate size. If no DNA aggregate was visible, samples were centrifuged at 13,000 g for 20 min to pellet DNA and water added to the pellet. Samples were incubated at 55°C until DNA dissolved (approximately 1 hour) and stored at -20°C until use.

Mice were genotyped by PCR amplification of mouse genomic DNA. Where relevant, the following primers; *CLEC-2*$^{+/+}$, *CLEC-2*$^{-/-}$ and common primers, R41A forward and reverse primers and R41 PF4-Cre forward and reverse primers (sequences listed in Table 1) were combined in the appropriate volumes with RedTaq®ReadyMix™ and Water PCR Reagent on ice to form a mastermix of which 19 µl was added to 1 µl of each genomic sample. Mixes containing genomic DNA for R41A and CLEC-2 were subject to the following PCR programme; 95°C, 5 mins, 95°C, 30 sec, 60°C, 30 sec, 72°C, 1 min, repeat steps 2-4 for 35 cycles, 72°C, 10 mins, 4°C forever. Mixes containing genomic DNA for PF4-Cre genotyping were subject to PCR programme, 95°C, 2 mins, 95°C, 30 sec, 56°C, 1 min, 68°C, 4 min, repeat steps 2-4 for 34 cycles, 72°C, 3 mins, 4°C forever. DNA bands were visualized using ethidium bromide on a 1.5% agarose gel.

2.3. Animal studies

All animal studies were conducted in accordance with Home Office protocols in compliance with project license 30/2721. All animal handling was done by a licensed individual.

2.31. Radiation chimera studies

2.311. Preparation of foetal liver cells

Foetal liver cells (previously prepared by Dr Craig Hughes, stored in 90% foetal calf serum and 10% dimethyl sulfoxide (DMSO)), derived from *CLEC-2*$^{+/+}$ or *CLEC-2*$^{-/-}$ mouse livers at embryonic days 14-16 were removed from liquid nitrogen storage, thawed at 37°C and re-suspended in an excess of Dullbeccos 1 X PBS. Cells were pelleted at 13, 000g for 5 min, supernatant removed and re-suspended in phosphate buffered saline (PBS) to give approximately 1-2 x 10^6 foetal liver cells per mouse.

2.312. Generation of chimeric mice

8 week old C57BL/8 mice (supplied by Harlan, UK) were kept on Baytil for one week before receiving two doses of radiation each 500 Rad, 3 h apart. Mice were then reconstituted by tail vein intravenous injection of 1-2 x 10^6 *CLEC-2* $^{+/+}$ or *CLEC-2*$^{-/-}$ foetal liver cells.

2.313. Platelet studies

Mice were culled at 1, 9, 21, 28 and 67 days post injection by inducing unconsciousness with isofluorane anaesthesia followed by CO_2 asphyxiation. The intestines of mice at 21 and 28 days were excised and photographed. At 9, 21, 28 and 67 days blood was drawn from the inferior vena cava into acid citrate dextrose (ACD) (1/9 vol), transferred into modified HEPES Tyrode buffer (134 mM NaCl, 2.9 mM KCl, 12 mM $NaHCO_3$, 0.34 mM NaH_2PO_4, 1 mM $MgCl_2$, 5.5 mM glucose, 1 mM $MgCl_2$, 20 mM HEPES [pH 7.3]) and taken for whole blood counts (ABX diagnostics). On days 9, 21 and 28, platelet rich plasma (PRP) was prepared by centrifugation (2 x 5 min spins at 2000 rpm) and diluted in HEPES Tyrode buffer to approximately 2 x 10^7 platelets/ml for flow cytometric analysis (FACS) (BD Biosciences) with antibodies against CLEC-2, CD41 and the respective IgG controls. Forward/side scatter gates were set to exclude non-viable cells.

2.314. Tissue harvesting and fixation

At 24 hr, the intestinal mesentery, intestine, liver and spleen were dissected, snap frozen in liquid nitrogen and stored at -80°C for cryosectioning. At 9, 21 and 28 days, the inguinal lymph nodes and intestinal mesentery were dissected and fixed (as described in 2.41) for whole mount immunostaining. Intestine, liver, spleen and mesenteric lymph nodes were dissected and embedded in O.C.T, snap frozen in liquid nitrogen and stored at -80°C for cryosectioning.

2.32. Harvesting and fixing CLEC-2 and R41A embryos

Pregnant females were culled at E 14.5 or E 16.5 by schedule 1 procedures, embryos removed into cold PBS and tail clippings taken for genotyping (see methods, 2.2). Embryos were gently removed from their membranes and photographed followed by fixing in 4% paraformaldehyde/PBS at 4°C for 90 min. Embryos were then cryoprotected in 20% sucrose/PBS overnight at 4°C. Embryos were snap frozen in liquid nitrogen and stored at -80ºC prior to cryosectioning into 8 µm sections.

2.4. Immunofluorescence staining

2.41. Whole mount

For whole mount immunostaining, tissues were directly fixed in acetone for 15 min; sections of intestinal mesentery at 21 and 28 days were spread over circular glass coverslips prior to fixing. Tissues were washed in PBS and incubated in 50 mM ammonium chloride for 30 min at room temperature (RT) with gentle shaking. Tissues were washed in PBS, 0.3% Triton X-100 (PBS-TX), blocked in 3% BSA/PBS-TX for 1 hour at RT followed by overnight incubation with gentle shaking at 4°C in primary antibodies to Lyve-1 and Endomucin (diluted in 3% BSA/PBS-TX). Tissues were washed extensively in PBS-TX and incubated overnight at 4°C with gentle shaking in secondary antibodies, IgG-FITC and Alexa Fluor®594, diluted in PBS-TX. Following extensive washing in PBS-TX, tissues were mounted onto a Colorfrost® Plus, charged microscope slide with a glass coverslip. Images

were obtained using a Leica SP2 confocal microscope using a 10X objective (0.3 Ph1) equipped with 488 and 543 lasers to excite FITC and Alexa Fluor®594, respectively. Images were processed using Adobe Photoshop 8.0.

2.42. Immunofluorescence of cryosections

For optimisation of immunostaining for cryosections, slides were removed from -80ºC and left at room temperature (RT) for 30 min or until dry. Where stated, sections were fixed in pre-cooled acetone at -20°C for 20 min. Following washing in PBS, 0.1% Tween (PBST), where stated, slides were quenched with 50 mM ammonium chloride and subsequently washed in PBST. Slides were blocked with 20% BSA/PBST or 10% goat serum in PBST, as stated in figure legends. Slides were incubated with primary antibody/antibodies, diluted in the relevant blocking solution, for 1 hour at RT (in dark where CD31-FITC applied) or overnight at 4°C followed by extensive washing in PBST. Slides were then incubated with secondary antibody/antibodies, diluted in the relevant blocking solution for 1 hour at RT in the dark followed by extensive washing in PBST. After 5 min incubation in the dark with To-pro-3-Iodide, diluted 1:2000, slides were washed extensively in PBST, left to dry at RT, mounted with Vectashield and stored at 4°C prior to confocal microscopy. Images were obtained using a Leica SP2 confocal microscope using a 10X (0.3 Ph1) or 40X oil objective (1.3 oil) equipped with 488 and 633 lasers to excite FITC and To-pro-3-iodide, respectively. Images were processed using Adobe Photoshop 8.0.

2.43. Immunohistochemistry

For immunostaining of paraffin sections, slides were de-waxed and dehydrated by immersion in xylene substitute (5 min), 100% ethanol (3 min), 90% ethanol (30 sec), 75% ethanol (30 sec), 50% (30 sec), 30% (30 sec), H_20 (3-5 min). Slides were then subject to the following antigen retrieval steps; Prox-1 treated slides were boiled in citrate buffer (2.94g Tris sodium citrate/1L water, 0.5% Tween, pH to 6) for 40 min. Podoplanin treated slides were microwaved in citric acid buffer (2.1g citric acid monohydrate/1L water, pH to 6) on full power for 3-4 min followed by 15 min on medium power. Slides were cooled to RT, washed in PBST and subject to an endogenous peroxidase block of 3% H_20_2 for 10 min at RT followed by further washing in PBST. Slides were blocked with 3% BSA/PBST for 1 hour at RT and then incubated overnight at 4°C with primary antibody, diluted in blocking solution. Slides were washed extensively in PBST before secondary antibody incubation, diluted in blocking solution, for 30 min at RT. Following extensive washing in PBST slides were incubated in VECTASTAIN® Elite® ABC Reagent for 30 min at RT followed by further washing in PBST before visualization with DAB substrate chromagen solution. Slides were counterstained in Harris' Haematotoxilin, dehydrated in 75% ethanol (3 min), 90% ethanol (3 min), 100% ethanol (3 min), xyelene substitute (1-5 min) and then overnight in xyelene substitute. Slides were dried off and mounted using VectorMount mounting medium. Images were obtained using a Zeiss Axiovert Zoom brightfield microscope using a 10X (0.3 Ph1) or 40X oil objective (1.3 oil). Images were processed using Adobe Photoshop 8.0.

2.44. TUNEL assay

TUNEL assays were performed according to the manufacturer's instructions on *CLEC-2*$^{+/+}$ E14.5 embryo cryostat sections and spleen, liver, intestine and mesenteric lymph node cryostat sections from *CLEC-2*$^{+/+}$ and *CLEC-2*$^{-/-}$ radiation chimeras. Slides were counterstained with To-pro-3-Iodide for confocal microscopy or with DAPI for widefield epi-fluorescent microscopy, diluted 1:2000 or 1:1000, respectively in PBS and incubated for 10 min at RT. Slides were washed extensively in PBS before mounting with Vectashield and stored at 4°C. For quantitative assaying, sections of spleen and livers from radiation chimeras were cut 20 µm apart, images taken on the widefield epiflourescent microscope and the percentage of apoptotic cells per DAPI stained nuclei calculated. Images were obtained using a Zeiss Axiovert Zoom invert epi-fluorescence microscope using a 40X oil objective (1.3 oil). Images were processed using Adobe Photoshop 8.0.

3.0. Results

3.*1. Genotyping and phenotyping R41A mice*

The generation of a megakaryocyte/platelet specific knock in mutation, R41A, within signalling molecule Syk was achieved through implementation of a loxP-Cre strategy utilising the PF4 promoter to direct expression of the mutated allele in the megakaryocyte lineage. Mice homozygous for the floxed allele, R41A$^{fl/fl}$ (Figure 2A and B, band 1) are crossed with mice expressing Cre recombinase from a PF4 promoter (Figure 2B, bands 3,4 and 5). Cre recombinase allows excision of the insert containing the wild-type R41 site flanked by the two lox P sites (Figure 2A) to allow expression of the Syk gene containing the R41A mutation within the megakaryocyte lineage (Ozgene). R41A mice were genotyped to accurately confirm the absence or presence of mutated (floxed) alleles in conjunction with the PF4-Cre expressing insert (Figure 2B).

The primary aim in researching the *R41A$^{fl/fl}$ PF4-Cre* mice was to characterise their developmental phenotype, in particular, observing any similarities and differences to the megakaryocyte/platelet specific *CLEC-2$^{-/-}$* mice (*CLEC-2$^{fl/fl}$ PF4-Cre)*. Figure 3 highlights the severity of the developmental defects observed at E14.5 in *R41A$^{fl/fl}$ PF4-Cre* embryos and the striking similarity to those seen at E14.5 in *CLEC-2$^{fl/fl}$ PF4-Cre* embryos. Both *R41A$^{fl/fl}$ PF4-Cre* and *CLEC-2$^{fl/fl}$ PF4-Cre* embryos presented with severe oedema, haemorrhaging in the brain and blood filled lymphatic vessels (Figure 3).

3.2. Optimising protocols for immunostaining

3.21. Immunohistochemistry of paraffin sections

In order to practice the immunostaining technique, a protocol for podoplanin immunohistochemistry which had previously been optimised in the lab was used to stain both *CLEC-2*$^{+/+}$ and *CLEC-2*$^{-/-}$ mouse adult lung paraffin sections. This demonstrated that *CLEC-2*$^{+/+}$ mouse lungs appeared much more developed and equipped for gas exchange as oppose to *CLEC-2*$^{-/-}$ mouse sections which appeared under-developed, likely contributing to the embryonic lethality of these mice (Figure 4A). Despite this observation, both *CLEC-2*$^{+/+}$ and *CLEC-2*$^{-/-}$ mice display the same developmental progressive expression of podoplanin in larger airways as they become adapted for gas exchange (Figure 4A). Additionally, only in *CLEC-2*$^{-/-}$ mice was there evidence for blood cells residing in lymphatic vessels, supporting the blood, lymphatic mixing phenotype and defective lymphatic vasculature commonly associated with this mutation (Figure 4B).

A key interest associated with this project, to be discussed later in the text, was the effect of *CLEC-2*$^{-/-}$ platelets on lymphatic vessel recovery in response to damage. It was therefore desirable to develop an efficient immunohistochemistry protocol for the LEC marker Prox-1, given the incomplete lymphatic specificity of the currently used LEC marker, Lyve-1[26]. However, the Prox-1 antibody (Abcam) proved to be highly temperamental and a variety of adaptations from the podoplanin immunohistochemistry protocol were trialled with only a few successful staining results (Figure 5), which occurred inconsistently. The main obstacle here

was considered to be the antigen retrieval steps where sections had to be subject to significant and extended boiling times.

3.22. Immunofluorescence of frozen sections

In light of these results it was decided to use frozen sections where proteins remain in their correct configuration for antigen binding. Since immunofluorescence of frozen sections was a new technique to the lab, a variety of protocols were attempted using a number of different antibodies of interest. No specific staining was observed for podoplanin, Prox-1 (Angiobio - chosen for increased suitability for immunofluorescence) or ephrin B4, a receptor tyrosine kinase with key roles in vascular development[27]. Consequently an antibody to pro-SPC, a transmembrane protein found in type I alveolar cells in the lung[28], known in the lab to work effectively for immunofluorescence staining of mouse adult lung sections, was tested to ensure the correct technique was being applied. Staining for pro-SPC was successful (Figure 6) and so at this point it was decided to interact with Professor Chris Buckley's lab (School of immunity and infection, University of Birmingham), who work effectively with immunofluorescence of frozen sections in order to develop a robust protocol for successful staining with the antibodies of interest.

Following protocol development, specific staining for CD31 was observed on both embryonic mouse cryosections and spleen and liver cryosections from radiation chimeras (Figure 7). However, immunofluorescence staining for podoplanin, Prox-1 and Lyve-1 required further enhancement to improve specificity. The inability at

this stage to reliably and reproducibly stain for a variety of antibodies of interest led to research into alternative assays that could be employed to investigate the extent of damage and recovery processes occurring in tissues of radiation chimeras.

3.3. Investigating damage and recovery processes in radiation chimeras

A pilot study was conducted to investigate the damage caused by radiation in different tissues to enable comparisons of recovery processes in mice reconstituted with *CLEC-2*$^{+/+}$ or *CLEC-2*$^{-/-}$ foetal liver cells (Figure 8).

3.31. Platelet studies

Analysis of platelets at 9, 21, 28 and 67 days post radiation and reconstitution, show as expected, both *CLEC-2*$^{+/+}$ and *CLEC-2*$^{-/-}$ mice were initially severely thrombocytopenic (64-144 x10^3/µl) and recovered towards having platelet counts within a normal range (900-1600 x10^3/µl) by 28 days (Figure 9)[29]. Correspondingly, mean platelet volume (MPV) was highly increased at day 9 following radiation treatment (12-17 µm^3) highlighting the presence of immature platelets[30]. MPV for both *CLEC-2*$^{+/+}$ and *CLEC-2*$^{-/-}$ reconstituted mice returned to within the normal range (4-6µm^3) by 21 days outlining no significant differences between the two groups in platelet counts and MPV over time (Figure 9)[29].

Fluorescence activated cell sorting (FACS) analysis confirmed the presence of platelet populations in both *CLEC-2*$^{+/+}$ and *CLEC-2*$^{-/-}$ reconstituted mice, indicated

by the shift in CD41 (αIIb) staining, a major platelet glycoprotein, as compared to the IgG control (Figure 10). Conversely, CLEC-2 staining of platelets showed only mice reconstituted with *CLEC-2*$^{+/+}$ foetal liver cells were positive for CLEC-2 at 21 and 28 days, confirming the loss of CLEC-2 from the megakaryocyte lineage in mice reconstituted with *CLEC-2*$^{-/-}$ foetal liver cells (Figure 10).

3.32. Phenotyping radiation chimeras

Prior to and during dissection, all mice were visually analysed and any differences between *CLEC-2*$^{+/+}$ and *CLEC-2*$^{-/-}$ chimeras were photographed. No visible adverse effects to radiation were observed prior to 28 days post reconstitution. At 28 days, the accumulation of blood in the intestine could begin to be seen in mice reconstituted with *CLEC-2*$^{-/-}$ foetal liver cells which was not visible in *CLEC-2*$^{+/+}$ chimeras (Figure 11A). It has previously been noted at 8 weeks that megakaryocyte/platelet specific *CLEC-2*$^{-/-}$ mice show considerable accumulation of blood in the intestine (Figure 11B) (Finney et al, manuscript in preparation).

Following on from the difficulties experienced in optimising immunofluorescence of frozen sections, whole mount staining was trialled on the inguinal lymph nodes and intestinal mesentery. Blood and lymphatic vasculature were visible at 9 days post radiation in the intestinal mesentery and appeared organised in *CLEC-2*$^{+/+}$ compared to *CLEC-2*$^{-/-}$ chimeras where vasculature seemed highly disrupted and damaged indicating a severe impairment of functionality (Figure 12).

High levels of background fluorescence in the inguinal lymph nodes and intestinal mesenteric sections at 21 and 28 days prevented images being taken for analysis despite the presence of visible, specific staining.

3.33. TUNEL labelling of apoptotic cells

In light of the difficulties experienced with immunofluorescence of frozen sections, alternative assays were considered to investigate the extent of damage over time in tissues most susceptible to radiation damage. The TUNEL assay was employed for specific labelling and detection of cells undergoing apoptosis (Figure 13).

TUNEL assays were trialled on spleen and liver cryosections from radiation chimeras 9 days post radiation and on *CLEC-2*$^{+/+}$ E14.5 embryo cryosections, known to encompass detectable levels of apoptotic cells due to the essential role of apoptosis in embryonic development[31]. The assay was performed according to the manufacturer's instructions and rigorous analysis ensured the correct alignment of rhodamine staining with To-pro-3-iodide stained nuclei (Figure 14). Positive TUNEL labelling was also visible in the intestine and mesenteric lymph nodes of radiation chimeras (data not shown).

To allow for quantification of the levels of apoptosis in the spleen and livers of radiation chimeras at various time-points following radiation, TUNEL labelling was performed on cryosections 20 μm apart and the percentage of apoptotic nuclei relative to DAPI stained nuclei were calculated. No substantial difference in the percentage of apoptotic cells between *CLEC-2*$^{+/+}$ and *CLEC-2*$^{-/-}$ chimeras were observed in liver cryosections. Additionally, although the number of apoptotic cells

were above the negligible number expected in the liver of a healthy animal, larger scale quantification is require to add significance to this observation[32]. In the spleen, heightened levels of apoptosis were seen in both *CLEC-2*$^{+/+}$ and even more so in *CLEC-2*$^{-/-}$ chimeras compared to levels (<2%) that would normally be expected (Figure 15)[33]. However, as this was a pilot study only two mice were available to be sacrificed at each time point, future studies should aim to increase this number along with the number of cryosections analysed per tissue and images per cryosection.

4.0 Discussion

4.1. R41A$^{fl/fl}$PF4-Cre embryos *phenocopy CLEC-2$^{fl/fl}$PF4-Cre* embryos

The mechanisms that co-ordinate the intricate separation of blood and lymphatic vasculature remain unknown. Mice deficient in the platelet receptor CLEC-2, experience defects in lymphatic development as early as E12.5. However, whereas constitutive *CLEC-2$^{-/-}$* mice are embryonically lethal, where CLEC-2 is specifically deleted from the megakaryocyte lineage, using the PF4-Cre strategy (*CLEC-2$^{fl/fl}$ PF4-Cre*), mice are viable and thrive after birth. As discussed, podoplanin deficiency results in a similar phenotype with blood/lymphatic misconnections. Since podoplanin on the surface of LEC's has been shown to induce potent platelet aggregation, it is speculated that CLEC-2 on platelets is directly involved in mediating the separation of blood and lymphatic vasculature[20].

R41A$^{fl/fl}$ PF4-Cre mice were generated to gain further insight into the role of CLEC-2 and signalling molecule Syk in blood and lymphatic separation through development. The R41A mutation specifically blocks Syk interacting with phosphorylated hemiITAM or ITAM receptors, hence ablating signalling[2]. Receptors such as integrins interact with Syk through alternative mechanisms and are able to signal through Syk and function as normal[5]. Like *CLEC-2$^{fl/fl}$ PF4-Cre* mice the *R41A$^{fl/fl}$ PF4-Cre* mice live to birth and future studies will aim to establish the mechanism behind this phenomenon which is likely to result from the varied activity of the PF4 promoter during development (Finney et al, manuscript submitted for publication).

Initial work in this area involved characterising the phenotype of *R41A$^{fl/fl}$ PF4-Cre* mice which appeared remarkably similar to that of the constitutive *CLEC-2$^{-/-}$* and *CLEC-2$^{fl/fl}$ PF4-Cre* mice at E14.5 where severe oedema, haemorrhaging in the brain and blood filled lymphatic vessels were visible (Figure 3). The blood filled lymphatic phenotype is common in mice with CLEC-2 signalling defects and is thought to result from the improper separation of blood and lymphatic vessels during development; the oedema observed is therefore a likely side-effect of the disrupted lymphatic vasculature, unable to efficiently conduct its drainage function[9]. Studies in PLCγ2 null embryos at E13.5, displaying a similar phenotype to *CLEC-2$^{-/-}$* embryos, reveal the aberrant separation of lymph sacs from the cardinal vein thus permitting blood flow into the lymphatic system[23]. Further work into locating and characterising the points of misconnection between blood and lymphatic vasculature is key towards determining the cause behind the blood filled lymphatic phenotype.

The development of subcutaneous haemorrhaging in the brains of *R41A$^{fl/fl}$ PF4-Cre* and *CLEC-2$^{fl/fl}$ PF4-Cre* embryos are not likely to derive from lymphatic dysfunction since the brain is absent of lymphatic vessels. Podoplanin expressing epithelial cells have been observed at the choroid plexus of the brain at sites which appear to localise with sites of bleeding[34]. Subcutaneous haemorrhaging has also been observed in both Syk and SLP-76 deficient embryos[21, 22, 35]. It is proposed that podoplanin expressing epithelial cells of the choroid plexus interact with circulating platelets to influence to formation of the blood-cerebrospinal fluid barrier in the brain through platelet signalling involving CLEC-2 and Syk (Finney et al, manuscript submitted for publication).

It is of interest to quantify the levels of CLEC-2 on the platelet surface through the course of development and through adulthood when it would be expected that the requirement of CLEC-2 in the separation of blood from lymphatic vessels would be diminished. Additionally, the wide tissue distribution of podoplanin implies the CLEC-2-podoplanin partnership may occupy additional, so far undiscovered roles[18].

4.2. Obstacles faced in optimising immunofluorescence of frozen sections

In preparation for investigating the damage and recovery processes in tissues of radiation chimeras, immunostaining protocols for a variety of antibodies of interest, for example, against antigens of the blood and lymphatic vasculature, were to be optimised.

Initial practicing of the immunohistochemistry technique employed a well-established protocol for podoplanin staining, leading to some interesting observations. The airways of the *CLEC-2*$^{+/+}$ lungs appeared well developed compared to those of constitutive *CLEC-2*$^{-/-}$ which were visibly under developed and appeared insufficient to allow viable gas exchange. Despite this lethal phenotype, the airways of *CLEC-2*$^{-/-}$ mice displayed the same progressive expression of podoplanin on type II alveolar cells as seen for *CLEC-2*$^{+/+}$ mice which is indicative of airways becoming viable for gas exchange. Recent work showed constitutive *CLEC-2*$^{-/-}$ mice presenting at birth with fluid accumulation in the lungs, severely reduced airspaces and abnormal lymphatic vascular patterning resulting in death shortly after birth (Finney et al, manuscript in preparation).

Similar pathology is seen in podoplanin deficient mice which are unable to inflate airspaces in the lungs after birth resulting in lethality[36]. Together these observations indicate the proper functioning of both podoplanin and CLEC-2 are required for viable lung development. During development, branching and morphogenesis are influenced by the secretion of fluid into the lumen of the lung from the airway epithelium[37]. The integrity of lymphatic vasculature in the lung is critical for the clearance of this fluid and likely underlies the inability of *CLEC-2*$^{-/-}$ and podoplanin deficient mice to inflate their lungs. This phenotype is not observed in megakaryocyte/platelet specific *CLEC-2*$^{fl/fl}$ *PF4-Cre* mice suggesting platelets only partly contribute to the defective lung development; alternatively, CLEC-2 on another cell types may be responsible for the observed lung phenotype (Finney et al, manuscript submitted for publication). Additionally, podoplanin stained blood filled LEC's were observed by neighbouring blood vessels which were not seen in *CLEC-2*$^{+/+}$ lung tissue, linking the role of CLEC-2 in blood and lymphatic vessel separation and the development of lethal lung pathology.

The difficulty experienced in optimising a protocol for Prox-1 staining in paraffin sections and the subsequent move to frozen sections brought new challenges as immunofluorescence of frozen sections was an unfamiliar technique to the lab. Individual antibodies require independent optimisation which can be timely and it is possible here that the desired antibodies used were not sufficiently suited for the immunofluorescence technique. Future work should involve further enhancement of blocking techniques to reduce background and employing signal amplification strategies to allow increased visibility of specific staining.

4.3. Investigating damage and recovery processes in radiation chimeras

Radiation is used widely in cancer treatment and as such the possible side effects and most vunerable tissues in man are well characterised to be the skin, gut, lymphoid organs and the liver[25]. The damage caused by radiation in the generation of chimeric mice is much less well documented and has generally been extrapolated from observations in humans. In most instances this is sufficient knowledge for the purpose of the study. However, recent studies comparing the recovery of lymphatic vessels post radiation between mice reconstituted with *CLEC-2*$^{+/+}$ or *CLEC-2*$^{-/-}$ platelets, outlined the need to establish the basal level of damage caused by radiation in chimeric mice (Barone, F et al, unpublished observations). This would allow for the direct association of the observed defects resulting from reconstitution with *CLEC-2*$^{-/-}$ platelets. In this short project a pilot study was conducted to begin to address this question.

4.31. No difference observed in platelet count recovery between CLEC-2$^{+/+}$ *and CLEC-2*$^{-/-}$ *chimeras*

As expected, platelet studies showed all chimeric mice were thrombocytopenic at 9 days post radiation and reconstitution confirming successful depletion of the bone marrow, lagging to replenish circulating platelets at a time point when the majority will have exceeded their life span[1]. Platelets present at 9 days had mean platelet volumes well above the normal range; these immature platelets are clinically symbolic post radiation treatment as the bone marrow is overwhelmed in its capacity to reconstitute the circulating haematopoietic niche[30]. Looking into the

activating capability of this initial platelet niche in response to different platelet agonists could have provided insight into the extent to which recovery processes are deferred. Both platelet count and mean platelet volume recover to the same degree in both *CLEC-2*$^{+/+}$ and *CLEC-2*$^{-/-}$ reconstituted mice as expected since CLEC-2 has no known role in platelet production and maturation. The absence of CLEC-2 on the platelets of mice reconstituted with *CLEC-2*$^{-/-}$ platelets was confirmed by FACS analysis.

4.32. CLEC-2$^{-/-}$ *chimeras show signs of a progressive intestinal phenotype*

It has previously been observed that irradiated mice suffer from substantial micro vascular endothelial cell death in the small intestine and hence, irradiation stimulates vascular repair in chimeras alongside replacing the hematopoietic cell niche[38]. Here, no significant adverse effects were observed prior to 28 days post radiation at which point the intestines of chimeric mice appeared notably more bloody in *CLEC-2*$^{-/-}$ chimeras. This supports the accumulation of blood in the intestine as being a progressive phenotype which becomes increasingly severe by 8 weeks in megakaryocyte/platelet specific *CLEC-2*$^{fl/fl}$ *PF4-Cre* mice (Finney et al, manuscript submitted for publication). Connections between blood and lymphatic vessels were observed in the intestines of PLCγ2 radiation chimeras which presented with blood and chyle ascites in the intestine. Interestingly, the observed blood-lymph shunts could be repaired following treatment with wild-type bone marrow cells, confirming the specific role of bone marrow derived cells in the vascular separation process[23]. Similarly, the intestinal phenotype observed in *CLEC-2*$^{-/-}$ chimeras was not seen in *CLEC-2*$^{+/+}$ chimeras suggesting the impaired

recovery to radiation damage results specifically from reconstitution with *CLEC-2*$^{-/-}$ foetal liver cells.

Interestingly, as early as 9 days post radiation, *CLEC-2*$^{-/-}$ chimeras appear to have more disrupted blood and lymphatic vasculature in the intestinal mesentery, visualised by whole mount staining. This mimics the loss of normal blood vessel architecture in the intestines of SLP-76 deficient radiation chimeras which was found to derive from blood/lymphatic misconnections[39]. In contrast, vasculature in *CLEC-2*$^{+/+}$ chimeras appeared organised and undamaged, indicating successful repair from radiation treatment. This suggests that the cause behind the intestinal phenotype discussed begins much earlier than visible. It can be speculated that *CLEC-2*$^{-/-}$ platelets are unable to repair the damage sustained by the vasculature from radiation treatment compared to *CLEC-2*$^{+/+}$ platelets which have the capacity to respond quickly to damage and initiate repair processes. It is however surprising that given the suggested incapability of *CLEC-2*$^{-/-}$ chimeras to respond to damage, that these mice do not show any additional obvious pathological side effects compared to *CLEC-2*$^{+/+}$ chimeras.

Future studies should look at later time points to investigate the intestinal phenotype further since it has been observed that damaging effects caused by radiation in *CLEC-2*$^{-/-}$ chimeras often become lethal by 12 weeks in contrast to *CLEC-2*$^{+/+}$ chimeras which commonly recover well (Finney et al, manuscript in preparation). Additionally, earlier time points are to be studied in megakaryocyte/platelet specific *CLEC-2*$^{fl/fl}$ *PF4-Cre* mice to enable further characterisation of when the phenotype manifests and how quickly it progresses.

4.33. Radiation induces elevated levels of apoptosis in liver and spleen

TUNEL assays were performed as a means of comparing the level of damage sustained by mice reconstituted with *CLEC-2*$^{+/+}$ or *CLEC-2*$^{-/-}$ platelets. TUNEL labelling is a widely used, robust assay to accurately label apoptotic cells, distinguishing them from the abundance of necrotic cells likely to be present in this scenario. Quantitative analysis of apoptosis in liver and spleen cryosections involved switching from confocal microscopy to widefield epiflouresent microscopy to allow quicker, more accurate analysis.

Although the levels of apoptosis in the liver appeared to increase above the negligible levels that would normally be expected[32], no substantial difference was observed. Apoptotic cells in the liver were largely individual and spread throughout the tissue, as represented in Figure 15Bii, indicating this tissue did not suffer extensive damage in response to radiation in either *CLEC-2*$^{+/+}$ or *CLEC-2*$^{-/-}$ chimeras.

It is stated in the literature that <2% of cells in the spleen undergo apoptosis under normal conditions[33]. With this in mind the data produced suggest a vast increase in apoptosis to what would normally be expected was observed in response to radiation damage in *CLEC-2*$^{+/+}$ and *CLEC-2*$^{-/-}$ chimeras. This is not surprising since the spleen is a hematopoietic organ holding a large number of radiosensitive, highly proliferating cells[40]. The increased levels of apoptosis observed in *CLEC-2*$^{-/-}$ chimeras potentially indicate a lag in recovery and sustained damage, however, since a decrease in the level of apoptosis is observed in both sets of chimeras at 28 days it is likely this difference not significant.

In order clarify these observations, future studies should include more early and extended time points as well as increasing the number of mice sacrificed to accurately monitor the change in apoptosis levels over time. It would also be preferable to increase the number of 20 μm separated cryosections and images taken per section to allow a more accurate representation of the level of apoptosis occurring in the tissue.

Crucially, quantitating apoptosis levels in the intestine, a tissue known to be highly radiosensitive during the early stages post radiation, could provide valuable information in relation the suspected progressive accumulation of blood observed in CLEC-2$^{-/-}$ chimeras.

5.0. Conclusion

The severe blood lymphatic mixing phenotype observed in both constitutive *CLEC-2*$^{-/-}$ and megakaryocyte/platelet specific *CLEC-2*$^{fl/fl}$ *PF4-Cre* and *R41A*$^{fl/fl}$ *PF4-Cre* embryos provides profound support for the role of platelet receptor CLEC-2 and signalling molecule Syk in the separation of blood and lymphatic vasculature. *CLEC-2*$^{-/-}$ radiation chimeras showed signs of a progressive intestinal phenotype by 4 weeks thought to derive from the impaired recovery of blood and lymphatic vasculature by reconstituted *CLEC-2*$^{-/-}$ foetal liver cells following radiation treatment. The role of platelets in the development of this phenotype is supported by the severe accumulation of blood in the intestine of megakaryocyte/platelet specific *CLEC-2*$^{fl/fl}$ *PF4-Cre* mice by 8 weeks along with previous reports of disrupted vasculature and blood filled intestines of SLP-76 and Syk deficient radiation chimeras. Although heightened levels of apoptosis were observed in the spleens of radiation chimeras, a highly haematopoetic organ, more work is required to determine the role of *CLEC-2* and Syk in the recovery from radiation damage.

6.0. Future directions

In addition to those already listed throughout this report, there are a number of aspects to radiation damage and recovery responses that would be interesting to study in future work.

Whole mount triple labelling for platelets (CD41), blood vessels (endomucin) and lymphatic vessels (Lyve-1) in the intestinal mesenteric tissue of radiation chimeras could provide an interesting viewpoint in visualising the integrity of the vasculature in *CLEC-2*$^{+/+}$ or *CLEC-2*$^{-/-}$ chimeras.

Quantifying the level of necrosis in different tissues would be of interest particularly at early time points when tissues such as the liver, spleen and intestine are likely to have sustained a high degree of damage. Assays are now available to study the number of normal, apoptotic and necrotic cells in concert (PromoKine).

A major obstacle in bone marrow transplantation comes with the phenomenon of 'graft versus host disease' (GVHD) where the host mounts a lethal immune response against the graft (donor cell line) leading to the development of severe secondary diseases (diarrhoea, skin changes, liver abnormalities etc) or even death. Monitoring the levels of T cell cytokines that promote GVHD progression (IL-2, IFN-γ); or measuring markers of inflammation, such as macrophages and inflammatory cytokines (e.g. TNF-α, IL-1), would help establish the extent of this reaction in different tissues[41].

Alternative pools of cytokines (e.g. colony stimulating factors) occupy essential functions in promoting proliferation of the surviving endogenous haematopoietic stem cells to direct their differentiation and functional maturity. Localising and

quantifying the abundance of these cytokines in different tissues may help assess the tissues capacity for recovery. For example, the spleen has been shown to become enriched with $CD4^+$ or natural killer cells which secrete cytokines to promote or inhibit haematopoiesis, respectively, in response to radiation[40]. Conducting this analysis alongside staining for proliferation markers such as ki67 would further investigate the regenerative capability of different tissues[42].

7.0. Figures

(A)

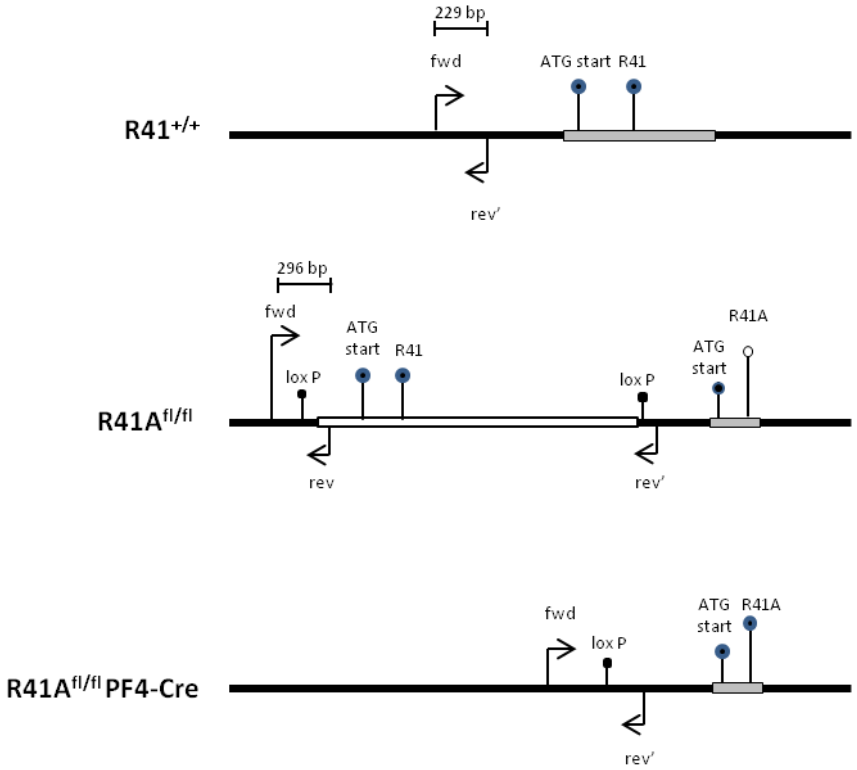

(B)

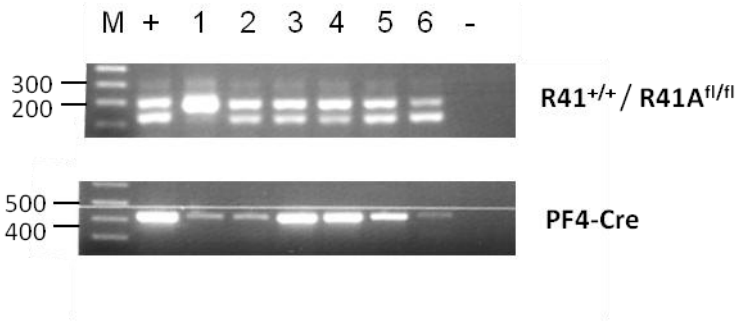

Figure 2. *Genetic strategy and genotyping of R41A mice.* (A) The $R41^{+/+}$ allele encompasses the Syk gene containing the R41 site downstream of an ATG start codon. The floxed (fl) allele, $R41A^{fl/fl}$, contains an insert (white box) including the $R41^{+/+}$ DNA flanked by two lox P sites upstream of second ATG start site and the R41A mutated codon. Amplification occurs preferentially from a second reverse primer site to give a 296 base pair (bp) fragment (plus a theoretical but unlikely 5015 bp fragment from primer rev'). When crossed with a PF4-Cre positive mouse, cre recombinase allows excision of the insert flanked by the two lox P sites to give the $R41A^{fl/fl}$*PF4-Cre* allele, specific to the megakaryocyte lineage (cannot be genotyped). Diagrams are not to scale. (B) R41A PCR; forward and reverse primers allow the amplification of a 229bp fragment from the $R41^{+/+}$ allele, and a 296bp fragment from the $R41A^{fl/fl}$ allele. PF4-Cre PCR; forward and reverse primers amplify a 400bp fragment confirming the presence of the cre recombinase cDNA insert. Molecular weight markers (bp) shown to the left. See Table 1 for primer sequences.

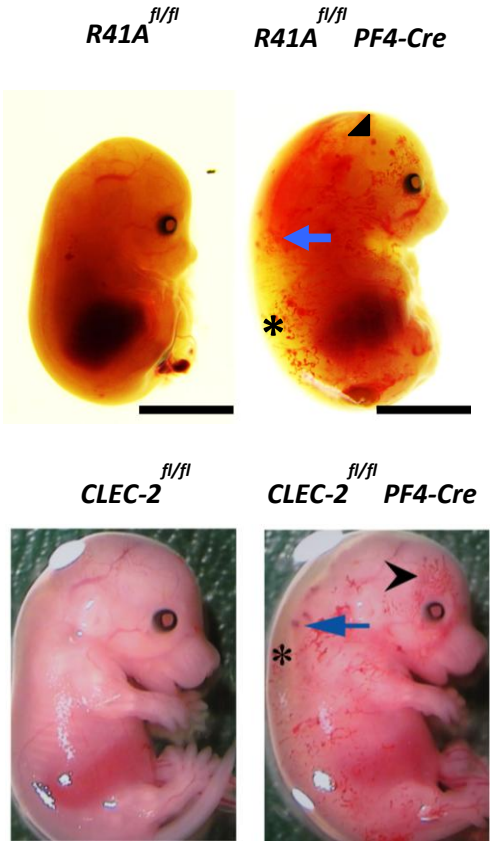

Figure 3. *Phenotyping R41A$^{fl/fl}$PF4-Cre and CLEC-2$^{fl/fl}$PF4-Cre embryos at E14.5.* Megakaryocyte/platelet specific *R41A$^{fl/fl}$PF4-Cre* embryos exhibit a similar phenotype to *CLEC-2$^{fl/fl}$PF4-Cre* embryos with severe oedema (stars), haemorrhaging in the brain (arrow heads) and bloody filled lymphatic spots (arrows). Mice homozygous for the flox allele (*R41A$^{fl/fl}$* and *CLEC-2$^{fl/fl}$*) do not exhibit this phenotype in the absence of PF4-Cre. (CLEC-2 images taken by Dr Brenda Finney).

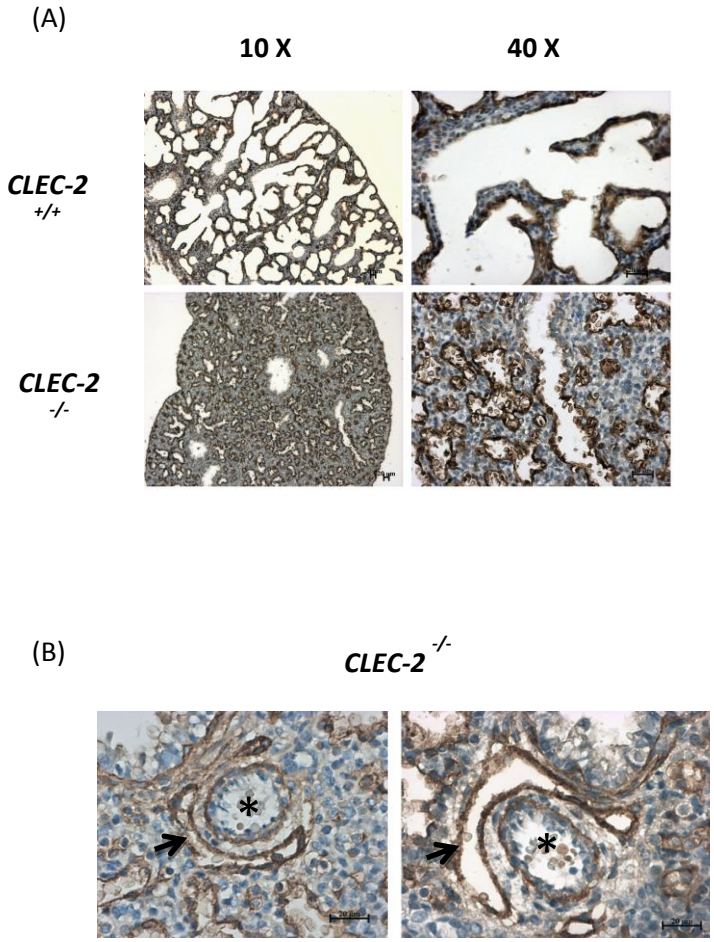

Figure 4. *Immunostaining for podoplanin in adult lung paraffin sections.* A and B show positive brown staining for podoplanin in type II alveolar cells (A) and LEC's (B). (A) Airways in *CLEC-2*$^{+/+}$ lung sections are well developed in contrast to *CLEC-2*$^{-/-}$ mice (10 X); progressive expression of podoplanin is observed in larger airways (40 X). (B) Podoplanin stained blood filled LEC's (arrows) around blood vessels (star) in *CLEC-2*$^{-/-}$ mice. All sections counterstained with Harris haematoxilin (blue). Scale bars represent 20 μm.

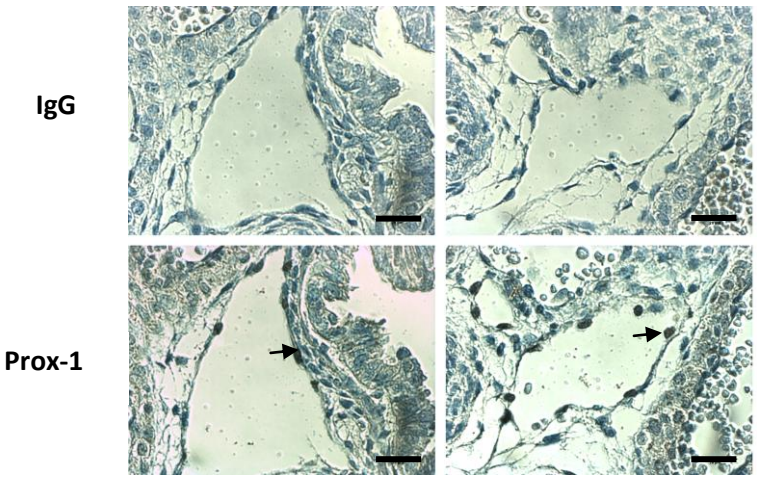

Figure 5. *Prox-1 immunostaining of LEC's in CLEC-2$^{+/+}$ lung paraffin sections at E16.5.* Prox-1 stained nuclei (arrows) line LEC's in the lung. No staining was visible when using IgG as a negative control. All sections were counterstained with Harris haematoxilin (blue). Scale bars represent 20 μm.

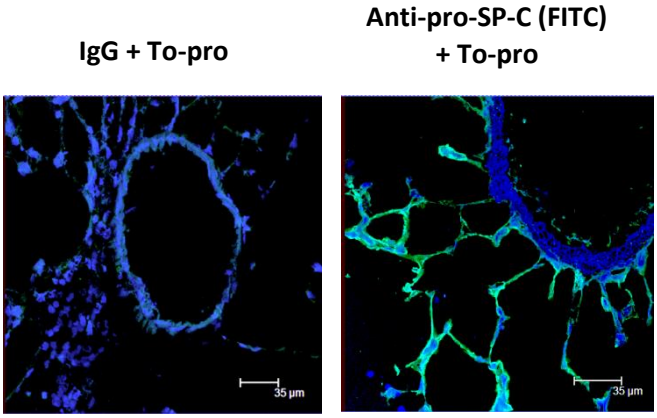

Figure 6. *Immunofluorescence of mouse adult lung sections with pro-SP-C.* Type I alveolar cells stained for pro-SP-C (FITC-green), no staining observed for the IgG negative control. Sections were quenched with ammonium chloride and blocked with 20% BSA/PBST. Nuclei counterstained with To-pro-3-iodide (blue). Visualised by confocal microscopy.

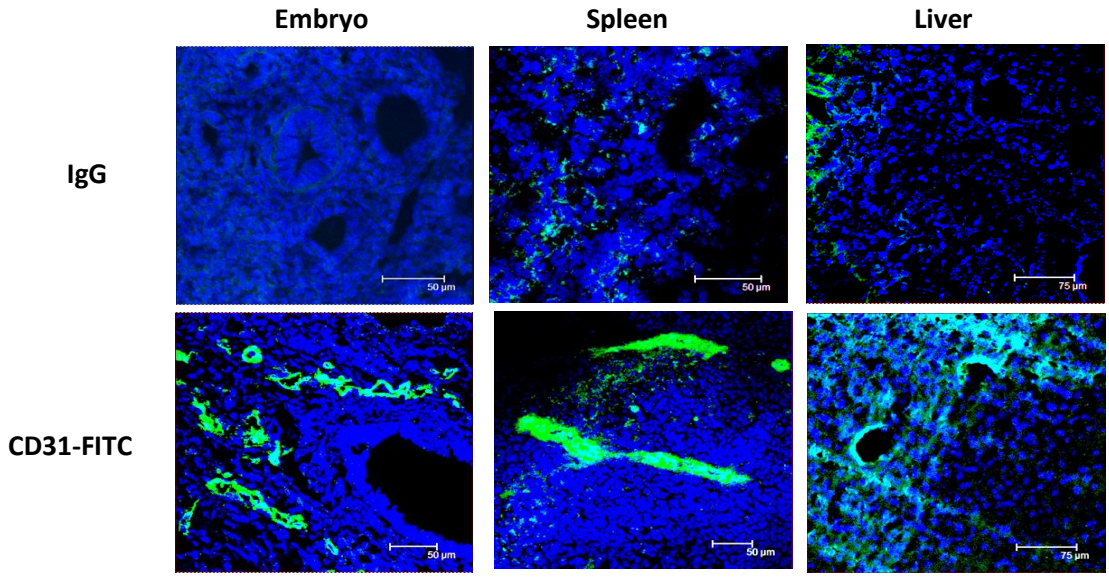

Figure 7. *Immunofluorescence of frozen sections with CD31-FITC.* Embryonic *CLEC-2*$^{+/+}$ mouse sections (E14.5), spleen and livers of *CLEC-2*$^{+/+}$ radiation chimeras (day 1) show positive CD31-FITC (green) staining of blood vessels in contrast to the IgG negative control. Sections were fixed in acetone and blocked in 10% goat serum/PBST. Nuclei counterstained with To-pro-3-iodide (blue). Visualised by confocal microscopy.

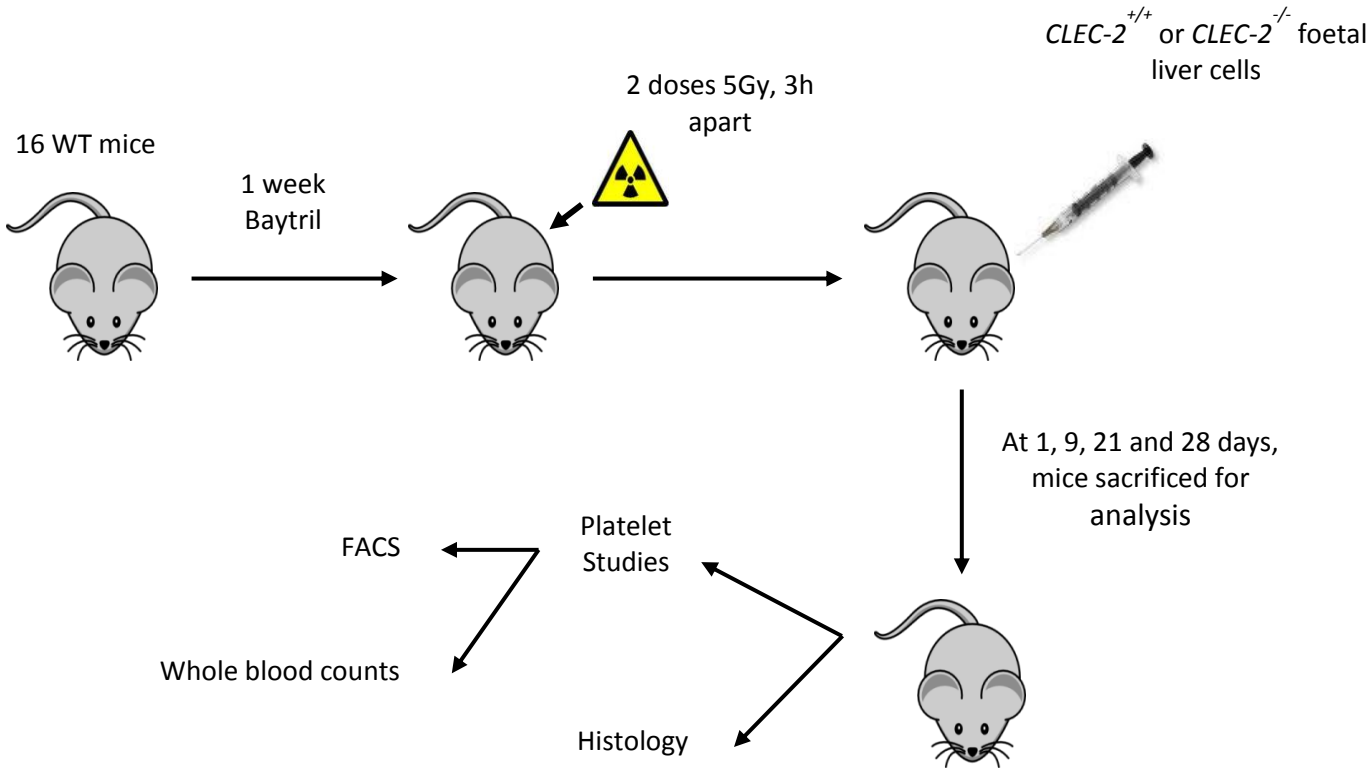

Figure 8. *Generation and analysis of radiation chimeras.* *CLEC-2*$^{+/+}$ mice were reconstituted with approximately 2 x 10^6 *CLEC-2*$^{+/+}$ or *CLEC-2*$^{-/-}$ foetal liver cells following irradiation induced depletion of the bone marrow. At various time points mice were sacrificed and blood and tissues taken for analysis.

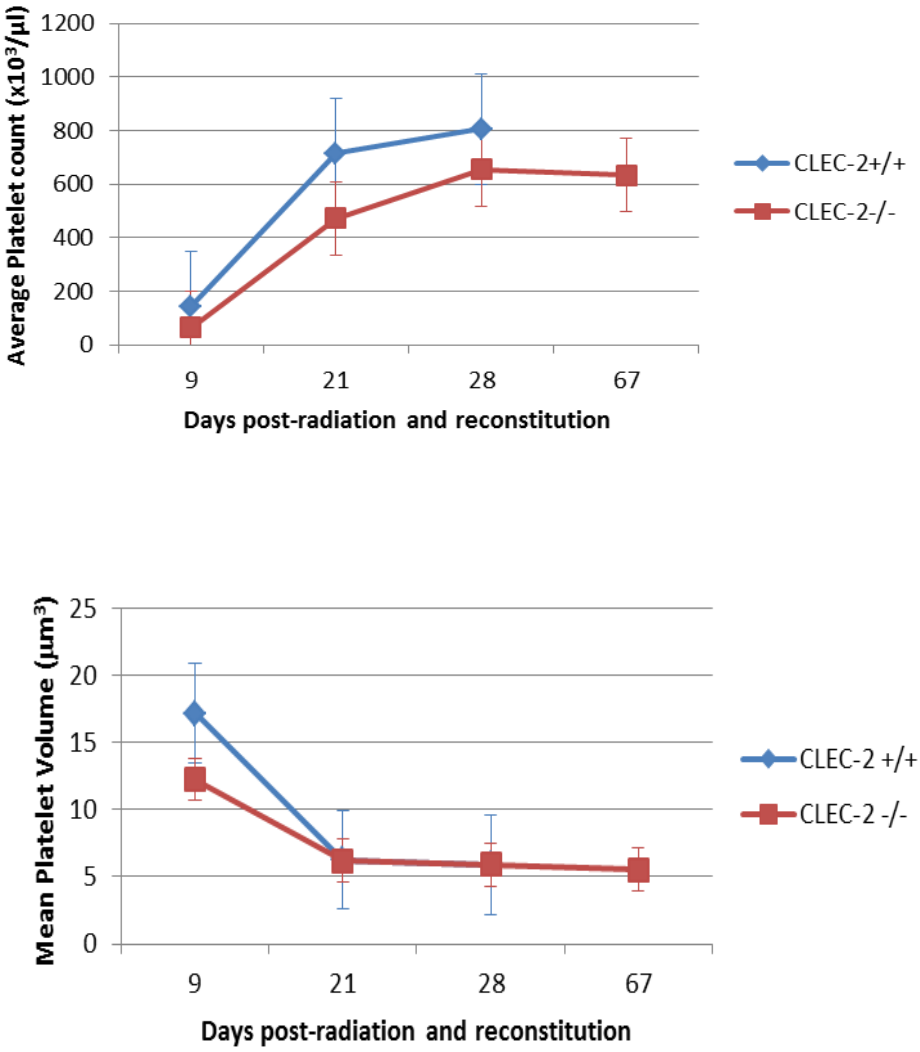

Figure 9. *Analysis of platelets in whole blood of radiation chimeras.* Platelets counts and MPV's were calculated from whole blood drawn from *CLEC-2*$^{+/+}$ and *CLEC-2*$^{-/-}$ chimeras at 9, 21, 28 and 67 (*CLEC-2*$^{-/-}$ only) days post radiation. Blood was transferred directly into ACD and transferred into HEPES Tyrode buffer (see methods 2.313). Each time point marks an average of blood from two mice where vertical bars indicate the standard error of the mean.

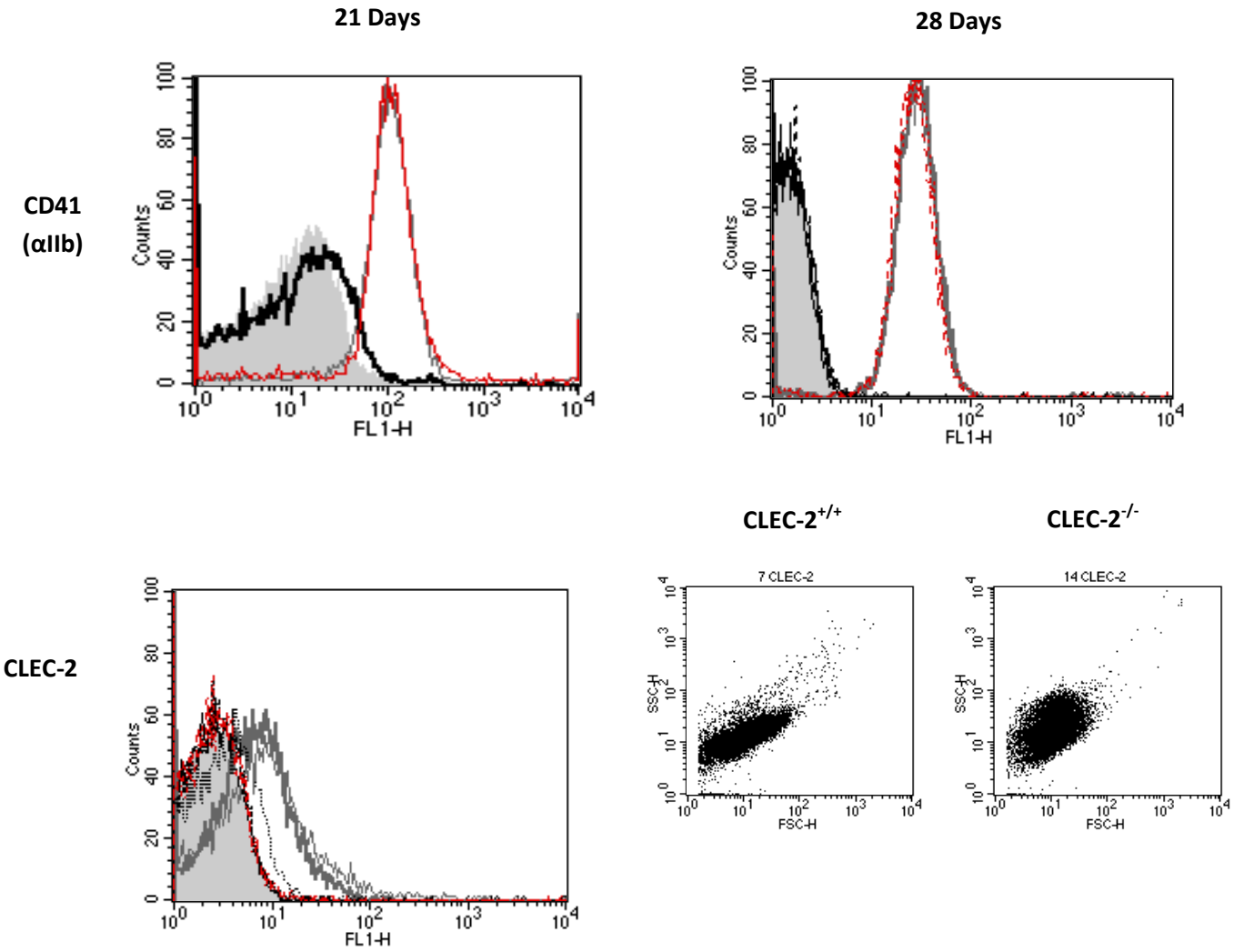

Figure 10. *FACS analysis of PRP at days 21 and 28 post radiation and reconstitution.* PRP was stained for CD41 and CLEC-2 (*CLEC-2*$^{+/+}$ chimeras, grey line, *CLEC-2*$^{-/-}$ chimeras, red line) along with IgG negative controls (*CLEC-2*$^{+/+}$ chimeras, grey fill, *CLEC-2*$^{-/-}$ chimeras, black line). For 28 days, CLEC-2 data is presented as scatter plots where a change in shape for *CLEC-2*$^{+/+}$ chimera PRP indicates platelet activation by the CLEC-2 antibody, not seen in PRP from mice reconstituted with *CLEC-2*$^{-/-}$ foetal liver cells.

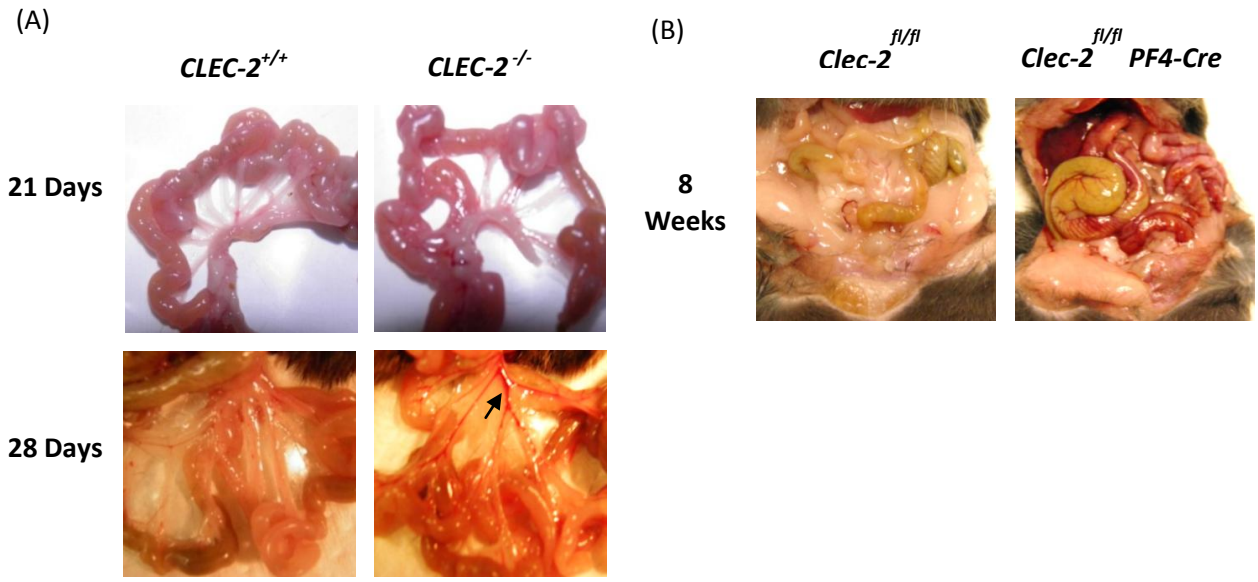

Figure 11. *Analysis of the intestinal phenotype in radiation chimeras.* (A) *CLEC-2*$^{+/+}$ and *CLEC-2*$^{-/-}$ radiation chimeras at 21 and 28 days post radiation and reconstitution; arrow indicates initial signs of accumulation of blood in the intestinal mesentery in *CLEC-2*$^{-/-}$ chimeras at 28 days. (B) Intestines of *CLEC-2*$^{fl/fl}$ mice appear normal compared to a notably more bloody intestine in megakaryocyte/platelet specific *CLEC-2*$^{fl/fl}$*PF4-Cre* mice at 8 weeks.

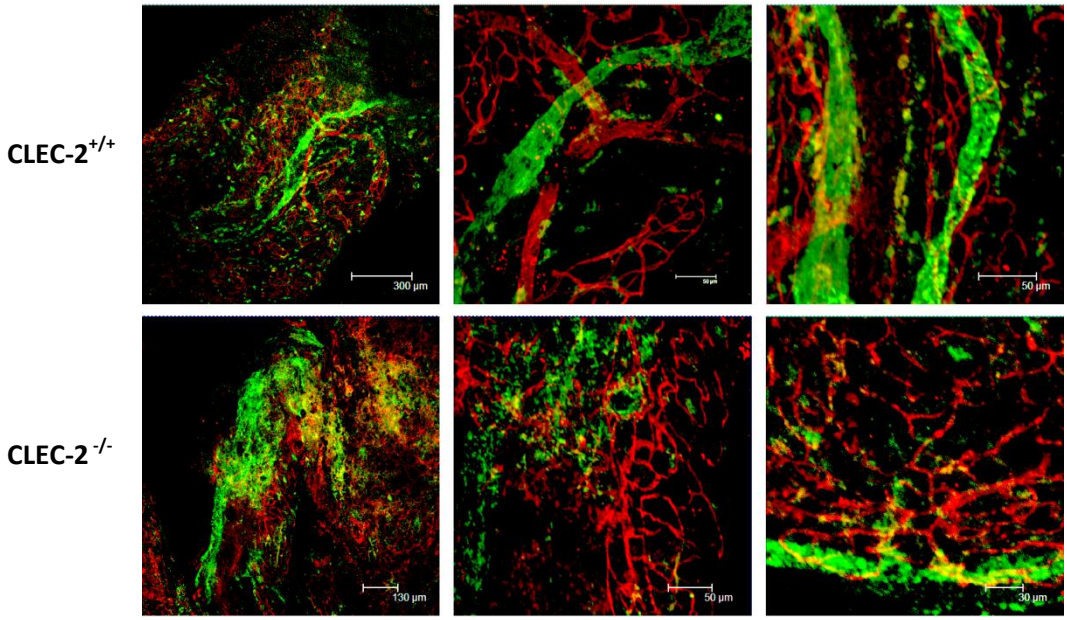

Figure 12. *Whole mount immunofluorescence staining of the intestinal mesentery.* The intestinal mesentery of radiation chimeras at 9 days post radiation and reconstitution with *CLEC-2*$^{+/+}$ and CLEC-2$^{-/-}$ platelets. Blood and lymphatic vessels stained with α-Endomucin (594-red) and α-Lyve-1 (FITC-green), respectively. Visualised by confocal microscopy.

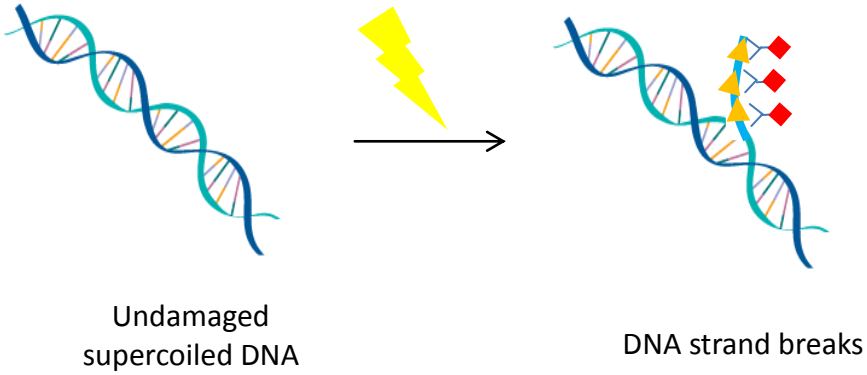

Figure 13. *Schematic diagram of the TUNEL assay technique for detection of apoptotic cells.* Digoxigenin labelled dNTP's (orange) are incorporated by TdT at the 3'OH of single and double strand breaks induced by radiation. Detection is through conjugation of an anti-digoxigenin-Rhodamine Ab.

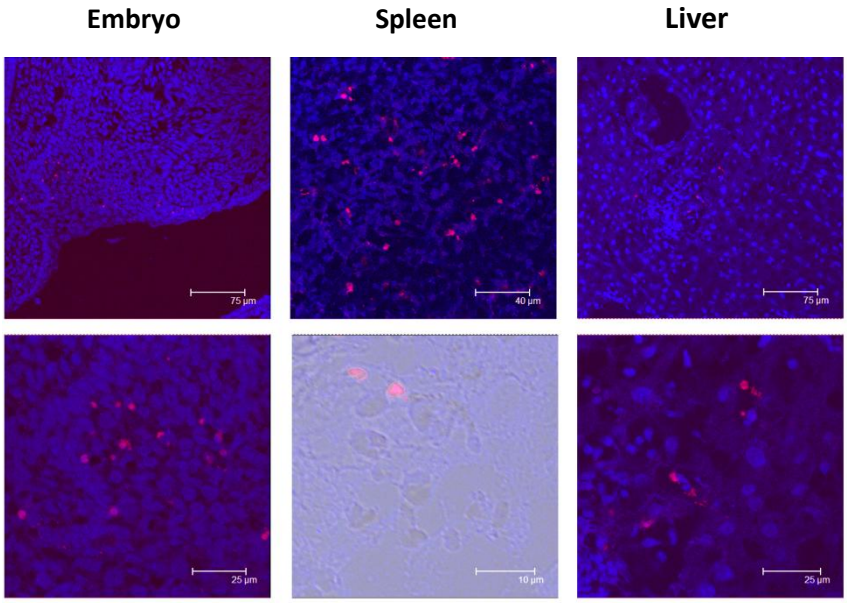

Figure 14. *Visualising rhodamine labelled apoptotic cells.* TUNEL labelling of apoptotic cells (red) in *CLEC-2*$^{+/+}$ E14.5 embryo cryosections and spleen and liver cryosections from *CLEC-2*$^{+/+}$ radiation chimeras 9 days post radiation and reconstitution. Images on the bottom panel are of higher magnification to show co-localisation of TUNEL labelled nuclei with To-pro-3-iodide (blue) stained nuclei. Visualised by confocal microscopy.

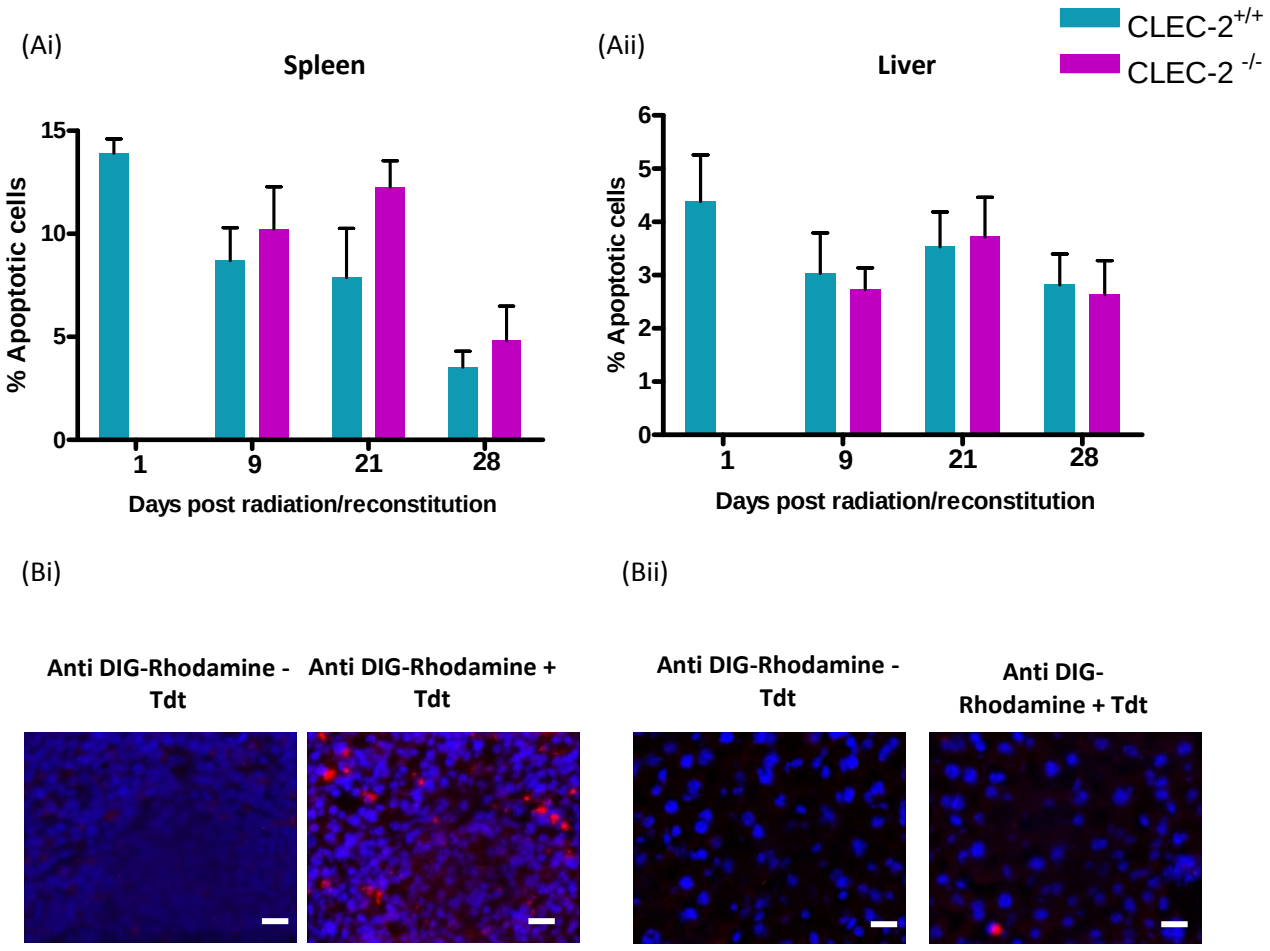

Figure 15. *Quantifying the level of apoptosis occurring in spleen and liver sections of radiation chimeras.* Three cryosections 20µm apart from *CLEC-2*$^{+/+}$only for day 1 and *CLEC-2*$^{+/+}$ and *CLEC-2*$^{-/-}$ radiation chimera tissues at 9, 21 and 28 days post radiation and reconstitution were TUNEL labelled and 3 images per section analysed by widefield epiflourescent microscopy for the number of apoptotic (red) and DAPI (blue) stained nuclei in one frame of view at 40 X magnification. The percentage of apoptotic cells relative to DAPI stained nuclei in spleen (Ai) and liver (Aii) are plotted. Representative images of negative control (-TdT) and TUNEL labelled spleen (Bi) and liver (Bii) cryosections are shown. Scale bars represent 20 µm.

	Primer Sequence (5’ to 3’)
CLEC-2$^{+/+}$ forward primer	GAT GAG TCT GCT AGG GAT GC
CLEC-2$^{-/-}$ forward primer	CAG AGG AAG AAA ACT CAG AAG G
CLEC-2 common reverse primer	AGC CTG GAG TAA CAA GAT GG
R41A forward primer	AGG CGG GGG AAT TAG AAG TTG AAG
R41A reverse primer	AGT CTT TGG ACA CAG TCC TCA AGG G
PF4-Cre forward primer	TGC ACA GTC AGC AGG TT
PF4-Cre reverse primer	CCC ATA CAG CAC ACC TTT TG

Table 1. *Primer sequences for CLEC-2$^{+/+}$, CLEC-2$^{-/-}$, R41A and PF4-Cre genotyping*.

A ROLE FOR ATRIAL NATIURETIC PEPTIDE IN PLATELET INHIBITION AND EVIDENCE FOR COMPARTMENTATION OF cGMP SIGNALLING

KATE LOWE

A thesis submitted to the University of Birmingham in part requirement for the award of MRes

Centre for Cardiovascular Sciences
Institute of Biomedical Research
College of Medical and Dental Services
University of Birmingham

August 2011

Abstract

Nitric oxide (NO) has long been accepted as a potent and powerful inhibitor of platelet function acting through soluble guanylyl cyclase (sGC) to elevate levels of cyclic guanosine 3',5'-monophosphate (cGMP). In cells such as cardiac myocytes, cGMP levels are also influenced by natriuretic peptides (NP) which bind to a particulate GC (pGC). Despite a number of studies indicating binding sites for atrial NP (ANP) on platelets, their influence on platelet function is unclear. Here it is demonstrated that NO and ANP mediate concentration-dependant inhibition of platelet aggregation to thrombin which is not overcome by high concentrations of the protease. ANP also stimulated weak phosphorylation of vasodilator stimulated phosphoprotein (VASP) in contrast to the robust response to NO and which was highly variable between donors. Further, sildenafil, a selective PDE5 inhibitor, was shown to enhance NO but not ANP mediated platelet inhibition and VASP phosphorylation indicating soluble and particulate cGMP pools are compartmentalised in platelets. Together these findings indicate a role for ANP in inhibiting platelet function which is distinct from that of NO.

Acknowledgements

Special thanks to Dr Melanie Madhani and Professor Steve Watson for supervising this project, to all members of the Birmingham platelet group for their help and support and to the Medical Research Council for funding this work.

Contents

1.0 Introduction 51

1.1. Background: Nitric oxide in regulating haemostasis 51

1.2. Regulation of NO signalling pathways in platelets 52

1.3. Inhibitory pathways of protein kinase G 54

1.4. Evidence for a pGC receptor on platelets 57

1.5. Compartmentation of cyclic nucleotide signalling pathways 59

1.6. Aims of the study 60

2.0. Methods 61

2.1. Reagents 61

2.2. Preparation of human platelets 61

2.3. Aggregation studies 62

2.4. Preparation of whole cell lysates 62

2.5. Western Blotting 63

2.5.1. Stripping membranes 64

3.0. Results 65

3.1. Investigating the expression of NPR-A on the platelet membrane 65

3.2. Comparing the inhibitory effects of NO donors and ANP on platelet aggregation 66

3.3. Comparing VASP phosphorylation in platelets treated with GSNO or ANP ... 68

3.4. Effects of the PDE5 inhibitor, sildenafil, on platelet aggregation and VASP phosphorylation 69

3.5. Effects of the non-specific PDE inhibitor, IBMX, on VASP phosphorylation ... 71

4.0. Discussion ... 72

4.1. Evidence for compartmentation of NO and ANP signalling in platelets ... 72

4.2. ANP mediates inhibition through VASP independent pathways ... 72

4.3. Evidence for thrombin stimulated PKG independant phosphorylation of VASP ... 75

4.4. ANP mediated platelet inhibition is not regulated by PDE5 ... 75

5.0. Conclusion ... 78

6.0. Future directions ... 79

7.0. Figures ... 80

List of Figures

Figure 1. Physiological factors influencing the inhibition and activation of platelets in the circulation 52

Figure 2. Production and regulation of cyclic nucleotides in platelets..... 56

Figure 3. Natriuretic peptide receptor topology and ligand binding specificities..... 58

Figure 4. Investigating the expression of NPR-A in platelets. 80

Figure 5. GSNO mediates concentration dependant inhibition of thrombin stimulated platelet aggregation..... 81

Figure 6. GSNO mediates concentration dependant inhibition of PAR-1 stimulated platelet aggregation. 82

Figure 7. DEANO mediates concentration dependant inhibition of thrombin or PAR-1 stimulated platelet aggregation. 84

Figure 8. ANP mediates concentration dependant inhibition of aggregation in thrombin and PAR-1 stimulated platelets. 86

Figure 9. GSNO mediated VASP phosphorylation in thrombin and PAR-1 stimulated platelets..... 87

Figure 10. Concentration and time dependent phosphorylation of VASP (Ser239) by GSNO and ANP..... 88

Figure 11. Sildenafil enhances platelet inhibition by GSNO but not ANP 90

Figure 12. IBMX enhances VASP phosphorylation in GSNO but not ANP treated platelets. 91

List of abbreviations

AC, adenylyl cyclase; ANP, BNP and CNP, atrial, brain and c-type natriuretic peptide; DEANO, diethylamine NONOate; HRP, horse raddish peroxidise; IBMX, 3-isobutyl-1-methylxanthine; GSNO, nitrosoglutathione; NO, nitric oxide; pGC, particulate GC; PDE, phosphodiesterase; PGI_2, prostacyclin; PAR-1, protease activating receptor-1; PKA, protein kinase A; PKG, protein kinase G; SERCA, sarcoplasmic reticulum ATPase; sGC, soluble guanylyl cyclase; TRAP-6, thrombin receptor activator peptide-6; TXA_2, thromboxane; VASP, vasodilator stimulated phosphoprotein.

1.0 Introduction

1.1. Background: Nitric oxide in regulating haemostasis

NO is produced in endothelial cells and constitutively released into the circulation where it has many essential roles towards controlling vascular tone, blood pressure and in regulating haemostasis. NO also acts alongside prostacyclin (PGI_2) to inhibit the activation of circulating platelets by elevating the levels of cAMP and cGMP, respectively[43]. Platelets express a vast array of surface receptors which are able to mediate rapid activation upon interacting with ligands such as thromboxane (TxA_2), thrombin or ADP (Figure 1). Platelet activation is associated with shape change through re-organisation of the cytoskeleton, secretion of vasoactive molecules, up-regulation of surface receptors, adhesion to subendothelial matrix, and aggregation resulting in thrombus formation[1, 44]. Acute regulation of both inhibitory and activatory pathways is essential for controlling platelet function.

.

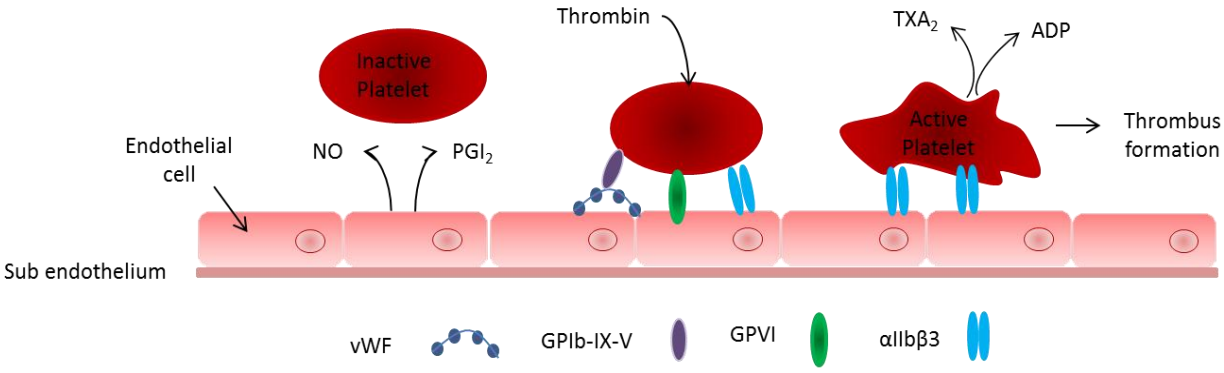

***Figure 1**. Physiological factors influencing the inhibition and activation of platelets in the circulation.* NO and PGI_2 released from endothelial cells maintain platelets in a resting state. Exposure of the subendothelial matrix leads to binding of VWF to collagen and tethering of platelets via the GPIb-IX-V complex. The low affinity collagen receptor GPVI is then activated leading to firm adhesion to the blood vessel wall as a consequence of integrin activation (e.g. $\alpha_{IIb}\beta_3$). The release of feedback molecules, ADP and TXA_2, promotes the recruitment of further platelets leading to aggregation and ultimately leading to thrombus formation. Adapted from Hoftbrand, Chapter 40[1].

1.2. Regulation of NO signalling pathways in platelets

NO is the most important inhibitor of platelet function and so, understanding the mechanisms behind its regulation and signalling pathways may help in the development of new anti-thrombotic therapeutic strategies.

NO stimulates sGC in platelets resulting in elevated levels of cGMP. cGMP acts synergistically to inhibit platelet function with cAMP, produced by adenylyl cyclase

(AC) which becomes activated upon interaction with a stimulatory G protein ($G\alpha_s$) released on receptor interaction with PGI_2 (Figure 2). The main targets of cGMP and cAMP are cGMP and cAMP-dependant protein kinases, also known as protein kinase G (PKG) and protein kinase A (PKA), respectively[45].

The levels of cyclic nucleotides are strictly regulated to enable the platelet to effectively perform its physiological function. Although cyclic nucleotides are primarily regulated by their synthesis, a key point of regulation is through their degradation. This is achieved by a family of PDE's which specifically hydrolyse cyclic nucleotides to produce biologically inactive 5' nucleotides[43]. A range of PDE's exist, each which vary in their subcellular location, mechanism of action and substrate specificity. In platelets, PDE 2, 3 and 5 are involved in regulating cAMP and cGMP levels and vice versa, through a complex web of interactions and feedback loops (Figure 2)[45]. For example, cGMP inhibits PDE3 to elevate levels of cAMP and enhance their inhibitory effect. The intricacy of the overlap between cAMP and cGMP signalling pathways is reflected their complex regulation by the PDE enzymes[46].

PDE inhibitors have been of great therapeutic interest as anti-platelet and anti-thrombotic tools, allowing temporary sustained elevation of cyclic nucleotides, hence inhibition of platelet activation and vasorelaxation. The successful formulation and application of a specific PDE 5 inhibitor was developed by Pfizer, Sildenfil (Viagra^{TM}) for treatment of erectile dysfunction[47].

1.3. Inhibitory pathways of PKG

PKA and PKG target several agonist induced pathways in platelets, including cytoskeletal reorganisation, integrin activation and elevation of intracellular calcium levels[43]. An agonist induced increase in cytosolic calcium levels results from the activation of phospholipase C (PLC) which stimulates the production of the inositol-1,4,5-trisphosphate (IP_3) receptor hence mediating the release of Ca^{2+} and subsequent activation of Ca^{2+} regulated proteins[48]. PKG-1 but not PKA has been shown to mediate inhibition of platelet activation through phosphorylation of the IP_3 receptor associated cGMP kinase substrate (IRAG), which is expressed in a macromolecular complex with PKG-1 and the IP_3 receptor type 1. Phosphorylation of IRAG by PKG-1 inhibits IP_3-induced Ca^{2+} release and, importantly, targeted deletion of the IP_3-binding region of IRAG prevents NO-mediated inhibition of platelet activation, whereas the inhibitory effect of cAMP is retained[49]. PKG has also been shown to act on the sarcoplasmic reticulum ATPase (SERCA) to stimulate the re-filling of intracellular Ca^{2+} stores[48].

Although the molecular mechanisms are unclear, the down regulation of Ca^{2+} release by cyclic nucleotides is thought to occupy an additional role in inhibiting platelet secretion, thereby inhibiting the release of activatory molecules such as integrin $\alpha_{IIb}\beta_3$, P-selectin and CD40 ligand[45]. PKG has additionally been shown to mediate phosphorylation of the TXA_2 receptor which prevents receptor coupling to the GTP binding protein, Gq, thus inhibiting activation of PLC[50].

Platelet proteins involved in cytoskeletal reorganisation that are thought to be potential substrates for PKA or PKG include heat shock protein 27 (Hsp27), myosin light chain kinase (MLCK), the GTPase, Rap1b and the vasodilator

stimulated phosphoprotein (VASP)[45]. The actin binding protein, VASP, is characterised as a prominent substrate for PKA/PKG in platelets where its phosphorylation correlates closely with inhibition of platelet aggregation[51]. VASP is a 50 kDa protein originally isolated in platelets but subsequently found to be expressed in a vast array of cells, including endothelial cells and T cells. VASP is an evolutionary conserved regulator of actin dynamics and is considered to have an array of physiological roles. In platelets, VASP is shown to localise to focal adhesion points where it is thought to occupy an anti-capping function to allow the extension of actin filaments[52, 53]. Three phosphorylation sites have been identified in VASP (serine 157, serine 239 and threonine 278). All three sites can be phosphorylated by PKA or PKG, although serine 157 and serine 239 are preferentially phosphorylated by PKA and PKG respectively[54]. VASP has been shown to influence the activation of integrin αIIbβ3 to disrupt fibrinogen binding hence inhibiting platelet aggregation[51]. The role of VASP as a negative regulator of platelet adhesion/aggregation is reflected in the enhanced exposure and activation of P selectin and αIIbβ3 in VASP deficient mice[55].

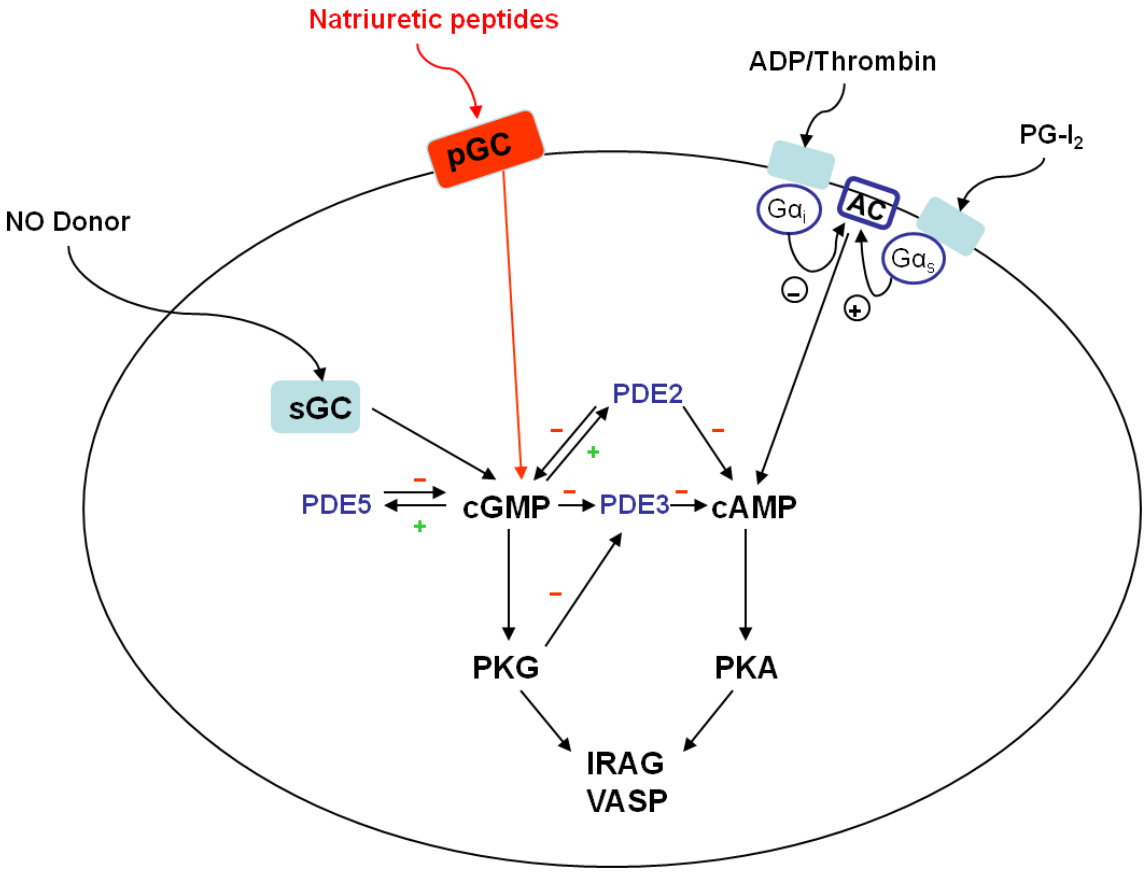

***Figure 2**. Production and regulation of cyclic nucleotides in platelets.* The main inhibitor of platelet activation, NO, directly activates sGC leading to the generation of cGMP and activation of PKG. PKG interacts with many substrates to influence platelet function, including, IRAG, VASP and PDE3 which hydrolyses cAMP. A second inhibitor of platelet activation, PGI_2 binds to a seven transmembrane protein coupled to Gs and thereby stimulates AC, increasing cAMP levels. Activatory stimuli such as thrombin and ADP also act through G proteins, releasing Gi and down regulating cAMP levels. cGMP is degraded by PDE5 and PDE2, negatively regulates PDE3 and positively regulates PDE5 and PDE2 to influence levels of cAMP which is degraded by PDE2 and PDE3. cGMP levels are also potentially influenced by natriuretic peptides (NP) binding to a pGC receptor. Adapted from Schwarz, 2001[45].

1.4. Evidence for a pGC receptor on platelets

In addition to sGC, cells such as cardiac myocytes have a cell membrane bound pGC receptor which is activated by the NP's, atrial NP (ANP), brain NP (BNP) and C-type NP (CNP)[46]. NP receptors (NPR) A and B possess intrinsic GC activity within their cytosolic domains allowing localised production of cGMP (Figure 3). In contrast, NPR-C functions independently of guanylyl cyclase and regulates local NP concentrations through receptor mediated internalisation and degradation. ANP, BNP and CNP can act as ligands for each of the NP receptors with the NPR-A having a higher affinity for ANP and BNP, and CNP having greater affinity for NPR-B. Similar to the role of NO, NP's have vital roles in the maintaining cardioprotective responses to ischemia, vascular tone and cardiac contractility[56].

It is currently unclear as to whether platelets contain a pGC receptor. Early work identified what was considered to be highly specific, yet reversible binding sites for ANP on platelets. However, ANP was shown to have no influence on cGMP levels and as such it was suggested that the receptor was not coupled to guanylyl cyclase[57]. This was supported by earlier work suggesting ANP had no significant physiological effect on platelet function[58]. This work was contradicted by Gear et al who proposed that ANP mediated an increase in cGMP levels in platelets which correlated with inhibition of platelet function; going on to suggest at least a proportion of ANP receptors on platelets are coupled to guanylyl cyclase[59]. It has also been suggested that ANP may contribute indirectly towards platelet inhibition by interfering with the inhibitory coupling of AC with agonist stimulation (e.g. ADP)[60]. More recently, platelets were confirmed to express NPR-C involved in the clearance and degradation of circulating natriuretic peptides but showed no effect

on intracellular cGMP levels in response to ANP[61]. More recent reviews refer to there being no pGC receptor on platelets but give no reference to support their conclusions[43, 45].

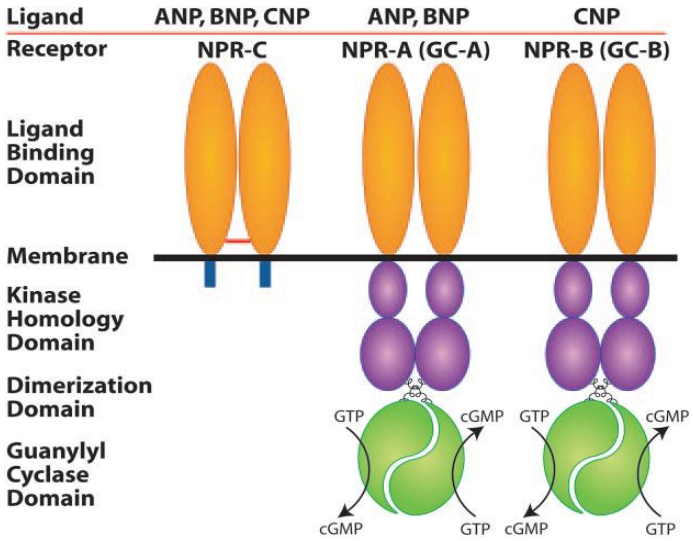

Figure 3. *Natriuretic peptide receptor topology and ligand binding specificities.* NPR-A and NPR-B have an extracellular ligand binding domain, single hydrophobic transmembrane domain, intracellular kinase, dimerization and guanylyl cyclase domains consisting of two active sites. NPR-C has only a 37 amino acid intracellular domain, however the extracellular ligand binding domain has approximately 30% homology to NPR-A and NPR-B. Figure taken from Potter et al[56]

1.5. Compartmentation of cyclic nucleotide signalling pathways

The idea that cyclic nucleotide signalling is compartmented in cells is becoming increasingly supported in the literature. The importance of this concept is reflected in the proposal that disorganisation in a cell, through the loss of compartmented signalling pathways reflects a disease state, for example, following heart failure[46].

Studies on cardiac myocytes for example, postulate that cells are able to distinguish between single stimuli acting on a specific signalling cascade. In this way, the spatial and temporal effects of cyclic nucleotides appear to be mapped by the co-ordinated distribution of protein kinases (PKA/PKG), PDE's, signalling proteins and their substrates[46, 62]. This concept can be extrapolated to platelets where it is postulated that signalling micro-domains, for example, at the platelet membrane or endoplasmic reticulum, may allow the effects of cGMP to be mediated without any significant change in global intracellular cGMP levels. PDE's have been of particular interest of late and are proposed to form signalling micro-domains within cells to direct a signal through specific signalling pathways[46]. This theory has been supported by Wilson et al who demonstrated the existence of a discrete microdomain in platelets, localised to Ca^{2+} channels. Within this microdomain, cGMP based control of Ca^{2+} release was regulated by the specific compartmentation of PDE5 with PKG[63]. Such local 'undetectable' changes in cGMP levels may allow tightened regulation of nearby Ca^{2+} channels and more transient changes to be effectively controlled. Adding to the complexity of NO signalling, sGC has been shown to translocate to the platelet membrane in response to agonist induced increases in intracellular Ca^{2+} where it becomes increasingly sensitised to NO, potentially to counteract the agonist response [64].

Membrane bound GC receptors form ideal localised domains for cyclic nucleotide signalling. It is postulated that pGC or sGC mediated elevation in cyclic nucleotides can have independent effects within a single cell such that, for example in cardiac myocytes, pGC activation works mainly to decrease intracellular Ca^{2+} levels while sGC signalling decreases Ca^{2+} sensitivity. If a similar situation exists in platelets, pGC could mediate signalling through alternative signalling pathways and mediate independent effects to sGC[62].

1.6. Aims of the study

The aims of the project are several fold:

i. Do platelets express a receptor for ANP
ii. Do platelets express a pGC receptor
iii. Does ANP mediate platelet inhibition and, if yes, is this mediated through pGC and how does the extent of inhibition compare to that of sGC
iv. Can inhibitors of PDEs be used to distinguish between pGC and sGC signalling?

2.0. Methods

2.1. Reagents

Primary antibodies used were rabbit anti-human Phospho-VASP (Ser239) (Cell Signalling Technology) and goat anti human NPR-A (Santa Cruz Biotechnology) and rabbit anti human NPR-A (Fabbgenix) were gifts from Dr Rob Fowkes, Royal Veterinary College, University of London. Secondary antibodies used were ECL™ donkey anti-rabbit IgG horse raddish peroxidase (HRP) (GE Healthcare) and donkey anti-goat IgG HRP (Santa Cruz Biotechnology). Additional materials used include Pierce® ECL western blotting substrate (Thermo Scientific), concentrated citrate solution, atrial natriuretic peptide (ANP), S-nitrosoglutathione (GSNO), isobutyl-1-methylxanthine (IBMX), diethylamine NONOate (DEANO) and thrombin (Sigma Aldrich), thrombin receptor activator peptide 6 (TRAP-6) (Altabioscience) and sildenafil citrate was a gift from Pfizer.

2.2. Preparation of human platelets

Whole blood was drawn from healthy volunteers into sodium citrate (1/10 vol) and further anti coagulated with acid citrate dextrose (ACD) (1/10 vol) to give a final citrate concentration of 3.8%. Platelets were obtained by centrifugation using PGI_2 (final concentration of 10 µg) to prevent activation during isolation. Washed platelets were re-suspended in modified HEPES Tyrode buffer (134 mM NaCl, 2.9 mM KCl,12 mM NaHCO3, 0.34 mM NaH2PO4, 1 mM MgCl2, 5.5 mM glucose, 1

mM MgCl2, 20 mM HEPES, and 5 mM glucose, pH 7.3) to a concentration of 2 X 10^8 platelets/ml for aggregation studies or 5 X 10^8 platelets/ml for western blotting.

2.3. Aggregation studies

Washed platelets (490 µl at 2 x 10^8 platelets/ml) were incubated at 37°C for 5 min. NO donors (GSNO or DEANO), ANP or phosphate buffered saline (PBS) were added and the sample was incubated at 37°C for a further 60 sec with stirring before stimulation with thrombin or TRAP-6. Where applicable, the PDE inhibitors, sildenafil (PDE5 inhibitor), IBMX (PDE2, PDE3 and PDE5 inhibitor) or control vehicle, 0.1 % dimethyl sulfoxide (DMSO), were added one minute prior to addition of NO donor or ANP. Aggregation was monitored by light transmission using Born lumi-aggregometer. Aggregation data is plotted as percent aggregation or percent inhibition of aggregation where 100 % represents maximal light transmission or maximal inhibition of light transmission, respectively. Points are mean values with standard error of the mean (s.e.m) shown by vertical bars.

2.4. Preparation of whole cell lysates

Washed platelets (290 µl at 5 x 10^8 platelets/ml) were left resting or stimulated as described (2.3) and samples lysed at different time points with 5 x sample buffer (10% sodium dodecyl sulphate (SDS), 25% 2-mercaptoethanol, 50% glycerol, 25% 0.5 M Tris HCl, pH 6.8, Brilliant Blue R, trance). Samples were immediately placed on ice before boiling at 100 ºC for 5 min and then stored at -20 ºC. Prior to

use, samples were defrosted thoroughly on ice and cellular debris pelleted by centrifugation (14, 000 x g for 3 min) at 4 ºC.

2.5. Western Blotting

Sample proteins were separated on a 12 % (Phospho VASP (Ser239)) or 8 % (α-NPR-A) SDS polyacrylamide gel in a Biorad tank with 1 X running buffer (0.025M Tris, 0.192 M Glycine and 0.1 % SDS) at 50 V through the stacking gel (stacking buffer; 0.5 M Tris-HCL, pH 6.8) and increased to 90 V through the resolving gel (resolving buffer; 3.0 M Tris-HCL, pH 8.8). Proteins were transferred to a PVDF membrane through a wet transfer method where the PVDF membrane and gel are sandwiched within a cassette in a Boriad tank. The central cassette is filled with transfer buffer (24 mM Tris, 191 mM glycine in 1:4 methanol:water) and the outer tank with water and transferred at 30 V for 90 minutes at 4°C. PVDF membranes were incubated in blocking solution (5 % bovine serum albumin (BSA), 0.1 % sodium azide in Tris buffered saline containing Tween 20 (TBS-T); 20 mM Tris base, 137 mM NaCl in distilled water, adjusted to pH 7.6 and 2 ml Tween 20 added) for 1 hour at room temperature or overnight at 4 °C. PVDF membranes were then incubated in primary antibody, diluted 1:1000 in blocking solution, for 1 hour at room temperature or at 4 °C overnight followed by 3 x 15 min washes in TBS-T. PVDF membranes were then incubated in secondary antibody, diluted 1:10000 in TBS-T, for 1 hour at room temperature or overnight at 4 °C followed by 3 x 15 min washes in TBS-T. Excess TBS-T was removed from membranes before immersion in ECL for 60 sec, membranes were wrapped in cling-film and placed protein side up into a film cassette. Hyperfilm was placed on top of the

blots within the cassette in the dark and exposed for the appropriate time before processing (Compact X5, Xograph imaging systems).

2.5.1. Stripping membranes

PVDF membranes were rinsed in methanol before stripping in stripping buffer (TBS containing 2 % Tween 20 and 2 % SDS) containing 0.1 % 2-mercaptoethanol for 20 min at 80 °C. Membranes were further incubated in stripping buffer alone for 20 min at 80 °C before washing in TBS-T. Membranes were blocked in 5 % milk powder in PBS containing 0.1 % Tween 20 (PBS-T) for 1 hour at room temperature. 0.05 % sodium azide was added to blocking solution and membranes incubated for a further hour at room temperature. Membranes were washed in TBS-T before incubating in primary antibody (α-NPR-A, Fabgennix) diluted in 5 % milk powder/PBST overnight at 4 °C. Membranes were washed 3 x 15 min in TBS-T before incubating in secondary antibody (donkey anti-rabbit HRP diluted 1:10000 in TBS-T) for 1 hour at room temperature. Membranes were processed as described previously in methods (2.5).

3.0. Results

3.1. Investigating the expression of NPR-A on the platelet membrane

The initial aim of the study was to identify whether platelets express a receptor for ANP and whether this receptor is coupled to GC. The pGC receptor, NPR-A, binds with greatest affinity to ligand ANP and has been shown to be highly expressed in kidney, adrenal, adipose, aortic and lung tissues[56]. NPR-A can be differentially glycosylated resulting in apparent molecular masses of 122 kDa or 130 kDa[65]. A band of this approximate size can be seen in a cardiac myocyte cell lysate western blotted for NPR-A (Figure 4). A series of bands running across the membrane, just below this are apparent in platelet lysates which may represent a less glycosylated form of the receptor (Figure 4). Different concentrations of ANP or its replacement with GSNO were included to observe any influence on receptor expression on the platelet. However, the high number of non specific binding sites of the NPR-A antibody make it difficult to firmly conclude the presence of the receptor on platelets. A second antibody (NPR-A, Fabgenix) to the receptor was applied to the membranes using an alternative protocol in attempt to enhance detection and reduce non specific binding, however, no bands of the expected molecular mass were observed (data not shown).

Given the uncertainty as to the expression of a receptor for ANP on platelets, alternative strategies were employed to investigate whether the peptide has any inhibitory effects on platelet function. Such analysis was to be performed alongside investigating the inhibitory effects of NO on platelets to allow relative comparisons.

3.2. Comparing the inhibitory effects of NO donors and ANP on platelet aggregation

Each of the NO donors within the vast array that are commercially available have varied effects across different tissues and in response to different agonists[66]. For this reason it was decided to investigate the inhibitory effects of two different NO donors, GSNO and DEANO in combination with two platelet agonists, thrombin and TRAP-6. Thrombin was selected on the basis of it being among the most powerful platelet agonists, mediating cleavage of the protease-activated receptors (PAR-1 and PAR-4) releasing a tethered ligand to bind and activate the receptor. TRAP-6, which will be referred to as PAR-1, is a synthetic peptide mimicking the binding sequence of the tethered ligand (serine-phenylalanine-leucine-leucine-arginine-asparagine)[1].

Thrombin induced maximal platelet aggregation at 0.03 u/ml (Figure 5A). Hence, this concentration of thrombin was taken as the threshold concentration for use in further experiments. Following pre-incubation with varying concentrations DEANO or GSNO, the extent of inhibition of platelet aggregation was determined. Platelet aggregation was only mildly inhibited at 0.1 μM and 1 μM GSNO with full inhibition of platelet aggregation being observed at 10 μM GSNO (Figure 5B and Ci). A ten-fold higher concentration of DEANO (100 μM) was required to consistently achieve maximal platelet inhibition (Figure 7A and 7Bi). When increasing the concentration of thrombin to 0.1 u/ml, the inhibitory effect of 10 μM GSNO or 100 μM DEANO was overcome and the ability of platelets to form aggregates restored (Figure 5Cii and 7Bii).

PAR-1 stimulated near maximal platelet aggregation at the threshold concentration of 10 μM and as such this concentration was taken for use in further experiments (Figure 6A). Both GSNO and DEANO mediated inhibition of platelet aggregation following stimulation with PAR-1 in a dose dependant manner, with a ten-fold lower concentration of DEANO mediating greater inhibition than was observed when stimulating with thrombin (Figure 6B, 6Ci and 7A, 7Ci). Reminiscent of the responses observed when stimulating with thrombin, when treating platelets with inhibitory concentrations of GSNO (10 μM) or DEANO (100 μM) aggregation could be restored when increasing concentrations of PAR-1 to 30 μM and 100 μM (Figure 6Cii and 7Cii).

Importantly, ANP was also observed to mediate concentration-dependant inhibition of platelet aggregation when stimulating with thrombin or PAR-1 (Figures 8A, Bi and Ci). Additionally, in contrast to what was observed with NO donors, platelet aggregation could not be restored when increasing thrombin or PAR-1 concentrations to 0.1 u/ml or 30 μM, respectively, following pre-incubation with 10 μM ANP (Figures 8Bii and Cii).

Higher variability was observed at the intermediate concentrations of NO donors or ANP potentially due to higher donor variability. GSNO was selected as a preferential NO donor for use in further experiments solely due to the lower concentration required to consistently mediate full inhibition of platelet aggregation.

3.3. Comparing VASP phosphorylation in platelets treated with GSNO or ANP

As discussed, VASP is phosphorylated by PKA and PKG preferentially at serine 157 and serine 239, respectively. Phosphorylation at serine 157 results in a mobility shift on an SDS-PAGE gel from 46 kDa to approximately 50 kDa, hence the two bands observed when immunoblotting with antibody phospho-VASP (Ser 239) (Figure 9). Control platelets, or platelets stimulated with thrombin gave no detectable levels of phospho-VASP (Ser239), with PAR-1 peptide inducing only weak phosphorylation at 1 and 3 minutes (Figure 9). Since the inhibitory effects or propensity to mediate VASP phosphorylation by GSNO were highly similar between thrombin or PAR-1 stimulated platelets, thrombin was selected for future experiments involving NO donors based on its greater physiological relevance.

When stimulating platelets with thrombin, a marginal increase in VASP phosphorylation was apparent (Figure 9 and 10A). Additionally, phospho-VASP (Ser239) levels appeared to peak at 1 min post stimulation with agonist (Figure 9 and 10A). Compared to the dose dependant increase in inhibitory effect of GSNO on platelet aggregation (Figure 5B), the intensity of bands indicative of phospho-VASP (Ser239) were seen to increase up to 1 µM GSNO where phosphorylation appeared to become maximal (Figure 10A).

Similar results were obtained from the same donor when pre-treating platelets with ANP. In the absence of thrombin, ANP mediated a concentration dependant increase in VASP phosphorylation, albeit bands appeared to be of significantly lower intensity to those derived from GSNO treated platelets. No difference in phospho-VASP (Ser239) levels were visible between 1 and 3 min post stimulation

with thrombin which appeared to become maximal above 0.1 μM ANP (Figure 10B).

The variable effects NO has within platelets derived from different donors is shown by the enhanced response to GSNO observed in figure 10C where maximal intensity bands for phospho-VASP (Ser239) are observed at a tenfold lower concentration of GSNO (0.1 μM) to what was seen in figure 10A. In this instance, ANP was shown to cause minimal or no VASP phosphorylation in thrombin stimulated platelets and even appeared to dampen down GSNO mediated VASP phosphorylation (Figure 10C).

3.4. Effects of the PDE5 inhibitor, sildenafil, on platelet aggregation and VASP phosphorylation

PDE5 is a key regulator of cGMP levels in platelets. Inhibition of PDE5 by pharmacological agents such as sildenafil, have been shown to effectively enhance the effects of cGMP. Here, platelet aggregation in response to treatment with sildenafil and in combination with GSNO or ANP was assessed in attempt to further investigate a possible signalling pathway for ANP and additionally establish any evidence for compartmentation of cyclic nucleotide signalling in platelets.

No effect on platelet aggregation was observed in platelets pre-treated with increasing concentrations of sildenafil (0.01 μM to 10 μM) prior to stimulation with thrombin (Figure 11A). When sildenafil was applied in combination with a fixed, sub maximally inhibitory concentration of GSNO (0.1 μM), platelet aggregation was largely inhibited an effect that was enhanced with increasing concentrations

of sildenafil (Figure 11A and Bi). In contrast, sildenafil did not enhance inhibition of platelet aggregation when in combination with a submaximal inhibitory concentration of ANP (0.1 μM) (Figure 11A and Bii). The slightly attenuated inhibition of platelet aggregation with 0.1 μM ANP compared to that seen in figure 8A may result from the marginal increase in thrombin concentration (0.05 u/ml compared to 0.03 u/ml used previously) used to stimulate the platelets. The increase in thrombin concentration was used to give reproducible platelet aggregation in a given donor platelet sample which was slightly less responsive to thrombin and was used thereafter for consistency.

Interestingly, non-treated platelets stimulated with thrombin gave rise to a significant level of phospho-VASP (Ser239) (Figure 11C). The extent of phosphorylation in thrombin stimulated platelets pre-treated with sildenafil increased minimally with rising concentrations of sildenafil. However, the inherent contribution of thrombin stimulated VASP phosphorylation is likely to have had a major influence towards the observed band intensities. Sildenafil enhanced the levels of phospho-VASP (Ser239) compared to platelets treated with sildenafil or GSNO alone, supporting their combined inhibitory effect on platelet aggregation.

As observed previously (Figure 10C), no phospho-VASP (Ser239) was seen in platelets treated with 0.1 μM ANP alone. When applied in combination with sildenafil, no enhancement in phospho-VASP (Ser239) was apparent relative to platelets treated with sildenafil alone. These data support the negligible effect of sildenafil in combination with the sub maximally inhibitory concentration of ANP (0.1 μM) on platelet aggregation. ANP appeared to suppress VASP (Ser239)

phosphorylation in thrombin stimulated platelets treated with 10 μM sildenafil but had no visible effect when combined further with GSNO (Figure 11C).

3.5. Effects of the non-specific PDE inhibitor, IBMX, on VASP phosphorylation

Since the effects of PDE5 inhibitor sildenafil appeared minimal towards enhancing the effects of ANP, it would suggest that if ANP is mediating platelet inhibition through cGMP/cAMP, an alternative PDE would be involved in regulating its actions. The non specific PDE inhibitor, IBMX, inhibits the activity of PDE2, PDE3 and PDE5, the three known platelet PDE's and hence was employed to further tease out a potential role for ANP in cyclic nucleotide signalling. IBMX has been used previously in platelets at concentrations ranging from 10 μM to 1000 μM[67, 68]. Here 150 μM was selected for use based on studies in cardiac myocytes where this concentration was sufficient to enhance ANP-induced inhibitory responses[69].

Although GSNO mediated VASP (Ser239) phosphorylation was significantly enhanced in combination with IBMX, little effect was observed in combination with ANP, potentially due to the observed negligible basal contribution of ANP towards phospho-VASP (Ser239) levels (Figure 12).

4.0. Discussion

4.1. Evidence for compartmentation of NO and ANP signalling in platelets

Bands running at the approximate size of an unglycosylated form of NPR-A (119 kDa) were visible in platelet lysates. However, the high levels of background and low specificity of the NPR-A antibody meant it was not possible to confirm the presence of a pGC receptor on platelets in this study. Alternative strategies were employed to investigate any inhibitory effect of ANP on platelet function. Characterising NO-induced platelet inhibition was a key control for relatively analysing any ANP-induced inhibitory effects.

ANP was shown to mediate irreversible inhibition of platelet aggregation at the maximal inhibitory concentration of 10 µM, leaving platelets unable to respond and aggregate to increasing concentrations of agonist. Conversely, although NO donors, GSNO and DEANO mediated similar dose dependant inhibition of platelet aggregation, aggregation could be effectively restored with increasing concentrations of agonist showing platelets remained responsive. This gives the first evidence in this study that NO and ANP signalling are compartmented in platelets allowing independent inhibitory effects on platelet function.

4.2. ANP mediates inhibition through VASP independent pathways

ANP was shown predominantly not to mediate VASP phosphorylation and where observed, phosphorylation was weak, suggesting VASP is not central to the

signalling pathway employed by ANP to mediate the observed inhibition of platelet aggregation. It has already been suggested that ANP may mediate platelet inhibition through an alternative mechanism to NO, a theory that is supported by the much lower levels of VASP (Ser239) phosphorylation comparative to GSNO treated platelets from the same donor. Possible mechanisms that are employed by NP's in other physiological systems, such as in smooth muscle relaxation, include the stimulation of Ca^{2+} channels at the membrane (e.g. $Ca^{2+/}$ATPase) or in intracellular compartments (e.g. SERCA) combined with inhibition of Ca^{2+} releasing receptors such as IP_3[56]. Thereby it be postulated that signalling by ANP could be compartmented to the plasma membrane or intracellular compartments to cause localised inhibitory effects. This is supported by work demonstrating the redistribution of PKG to the plasma membrane upon stimulation with ANP, where PKG directly interacts with NPR-A[70]. Additionally, in vascular smooth muscle cells, significantly lower levels of ANP were shown to activate cyclic nucleotide gated channels more rapidly than NO donors indicating ANP may perform unique actions to NO donors and compartmentation of ANP signalling may strategically enhance its inhibitory effects[69].

Where ANP appeared to cause a reduction in VASP (Ser239) phosphorylation in GSNO treated platelets (Figure10C), it can be speculated that ANP signalling through VASP independent pathways reduces the intensity of NO signalling as PKG becomes localised to discrete compartments. The irreversible inhibition of platelet aggregation previously observed at 10 µM ANP links the potential enhanced potency of compartmentalised cyclic nucleotide signalling to enable constitutive inhibition. Additionally, a phenomenon that is becoming increasingly documented and could account for the much greater suppression of VASP

phosphorylation observed at 10 μM ANP is the desensitization of GC receptors resulting from continued exposure to NP's. Desensitisation is caused by constitutive dephosphorylation of cytoplasmic residues in the kinase homology domain of NPR-A (Figure 3) rendering it inactive[71]. This analogy does not however link in with the irreversible inhibition of platelet aggregation observed at 10 μM ANP which would suggest receptors are constitutively active.

As mentioned, GSNO mediated high levels of VASP (Ser239) phosphorylation supporting the role of VASP in NO mediated inhibition of platelet aggregation. The slight increase in VASP phosphorylation in platelets treated with GSNO and further stimulated with thrombin, may reflect the ability of NO to respond rapidly to counteract platelet activation and lends itself to the idea that sGC is compartmented with its substrate VASP within the platelet to enable rapid propagation of signals.

Phosphorylation of VASP did not correlate directly with the GSNO dose dependant inhibition of aggregation such that above a threshold concentration, e.g. 0.1 μM GSNO (Figure 10C), phosphorylation appeared equivalent and sustained. This suggests that inhibitory substrates other than VASP contribute to the elevated inhibitory effect of GSNO at higher concentrations. For example, in rat platelets, the relative inhibitory effects of sGC vary between tissues and inhibition is thought to be largely through stimulation of calcium re-uptake into intracellular stores through activation of proteins such as sarco-endoplasmic reticulum calcium-ATPase SERCA[66].

4.3. Evidence for thrombin stimulated PKG independent phosphorylation of VASP

Interestingly, in some cases western blot analysis of non treated platelets stimulated with thrombin gave rise to significant levels of phospho VASP (Ser239). Phosphorylaion of VASP at Ser 157 has been observed previously in platelets stimulated with thrombin (Naseem, unpublished observations). It has been suggested that phosphorylation of VASP (Ser157) in response to thrombin may be derived from protein kinase C (PKC) and Rho kinase dependant pathways[54]. Here, the majority of thrombin induced VASP (Ser239) phosphorylation is seen at 46 kDa indicating minimal phosphorylation of Ser 157. One explanation for this comes from studies in human embryonic kidney (HEK-293) cells where PKC was shown to mediate phosphorylation and activation of PKG, hence allowing phosphorylaion of VASP (Ser 239)[72].

4.4. ANP mediated platelet inhibition is not regulated by PDE5

Comparative to what has been observed previously in platelets, sildenafil alone had no effect on platelet aggregation but enhanced the inhibitory effects of GSNO by sustaining the levels of cGMP[73]. This is also reflected by the increase in VASP (Ser239) phosphorylation in platelets treated with both sildenafil and GSNO. Increasing cGMP levels have been shown to synergise with elevated cAMP levels through the cGMP mediated inhibition of PDE3[74]. Since it is suggested that PDE3 is responsible for around 80 % of cAMP hydrolysis required to prevent platelet

aggregation, this is likely to be a key contributor to the observed inhibitory effect[75].

In contrast, sildenafil was shown to have no effect on platelet inhibition by ANP, with phospho-VASP (Ser239) band intensities of the representative samples resembling those of platelets treated with sildenafil alone. Such findings are in agreement studies in cardiac myocytes where the specific distribution of different PDE's have been found to play key roles in controlling pGC and sGC cGMP pools. It was observed that PDE5 is critically involved in controlling the soluble pool of cGMP yet dispensable for the particulate pool which it is said to be under the exclusive control of PDE2[62]. Conversely, PDE5 was shown to be a key regulator of cGMP-mediated vasodilation of blood vessels by ANP in the pulmonary but not systemic circulation, highlighting the critical complexity of regulation, highly determinant of the physiological environment[76]. The severely suppressed phosphorylation of VASP (Ser239) in platelets treated with 0.1 µM ANP and 10 µM sildenafil (Figure 11C), potentially results from allosteric activation of PDE2 resulting from a high concentration of sildenafil[75]. Since it has been suggested the pGC pool may be strictly regulated by PDE2, the drastic decrease in VASP (Ser239) phosphorylation correlates with a diminished particulate cGMP pool.

The apparent negligible contribution of PDE5 towards platelet inhibition and VASP phosphorylation by ANP suggests that if ANP signalling is directed through cGMP pools, they are not regulated by PDE5. The non-specific PDE inhibitor, IBMX was employed in attempt to further investigate any regulatory role of PDE's in ANP signalling.

IBMX significantly enhanced GSNO induced VASP (Ser239) phosphorylation further highlighting the importance of PDE's in regulating the soluble cGMP pool. Where ANP alone caused no visible phosphorylation of VASP, it is not surprising that in platelets treated with both ANP and IBMX, levels of VASP phosphorylation were representative of those treated with IBMX alone. Further work is required to assess the contribution of PDE's in regulating platelet inhibition through ANP. In cardiac myocytes it has been shown that PDE's have minimal influence in regulating the pGC cGMP pool and instead are under the strict regulation of PKG which positively regulates the pGC receptor[77].

It is also possible that ANP binds to NPR-C, a receptor shown previously to be present on platelets which has high affinity for ANP and has been seen inhibit AC activity[61, 78]. This correlates with the low levels of ANP induced VASP phosphorylation at serine 157 (50 kDa bands), a site which is predominantly phosphorylated by cAMP. The preferential phosphorylation of VASP at Ser239 by ANP have been noted in previous studies and suggest ANP signals through a PKG dependant mechanism[79]. The mechanisms by which NPR-C may influence cGMP pools are however unknown.

It is additionally entirely possible that given the inconsistent and minimal phosphorylation of VASP, ANP inhibits platelets by a cGMP independent mechanism. For example, cGMP analogs have been shown to cause rapid inhibition of thrombin, TXA_2 or vWF induced platelet activation through an unknown PKG independent mechanism[80].

5.0. Conclusion

Through functional analysis it is demonstrated that ANP can bind to platelets and mediate inhibition of platelet function. ANP and GSNO were shown to have differential effects on VASP, hence, it is proposed that if ANP signalling is cGMP dependant, soluble and particulate cGMP pools are compartmented, regulate different signalling pathways and are themselves, differentially regulated. For example ANP may mediate inhibition by controlling the activity of Ca^{2+} channels at the platelet membrane or endoplasmic reticulum regulated independently of PDE5. The irreversible inhibition of platelet aggregation and suppression of VASP phosphorylation by 10 μM ANP is an intriguing result that despite speculation remains unexplained yet supports the idea of compartmentation of ANP and NO signalling. Much more work over a vast range of donors is required to unravel a mechanism by which ANP mediates inhibition of platelets and the mode of its regulation.

6.0. Future directions

Determining the presence of a pGC receptor on platelets remains a key aim for future work. Protocol development strategies to enhance the specificity for detection of NPR-A are required. Additionally it is of interest to confirm the presence of NPR-C and quantitate the levels of the receptor on the membrane.

Unravelling the mechanism by which ANP mediates inhibition of platelet aggregation is a key future aim. Completing studies using IBMX as well as independent studies using an inhibitor of PDE2, for example, erythro-9-(2-hydroxy-3-nonyl)adenine or inhibitors of PKG, for example, KT5823, are crucial towards determining the involvement of cGMP and its mode of regulation[62, 77].

Applying an inhibitor of sGC, for example, ODQ (1*H*-[1,2,4]oxadiazolo[4,3-*a*]quinoxalin-1-one) and measuring the intracellular levels of cGMP using detection methods such as the cGMP enzyme immunoassay (EIA) kit (Cayman Chemicals) would enable the individual contribution of ANP to be quantified (d'Emmanuele di Villa Bianca, in press).

7.0. Figures

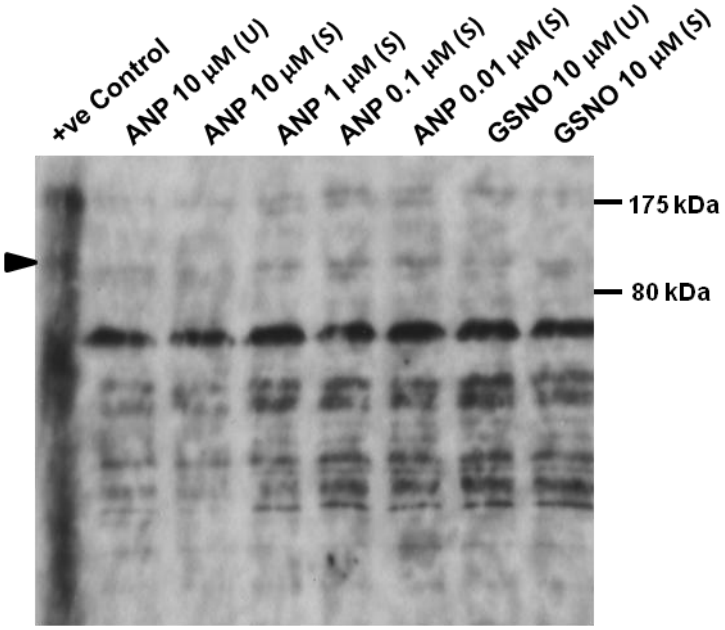

Figure 4. *Investigating the expression of NPR-A in platelets.* Positive (+ve) control of whole mount heart, 10% homogenate. For the remaining lanes, washed platelets (5 x 10^8/mL) were incubated with ANP or GSNO and stimulated with thrombin (S) or left unstimulated (U). Samples were lysed with 5 X sample buffer, proteins separated by SDS-PAGE and western blotted for α-NPR-A. Molecular weight markers indicated to the right. Block arrow to the left of the gel indicates a band at approximately 130 kDa in the +ve control lane. (n=2).

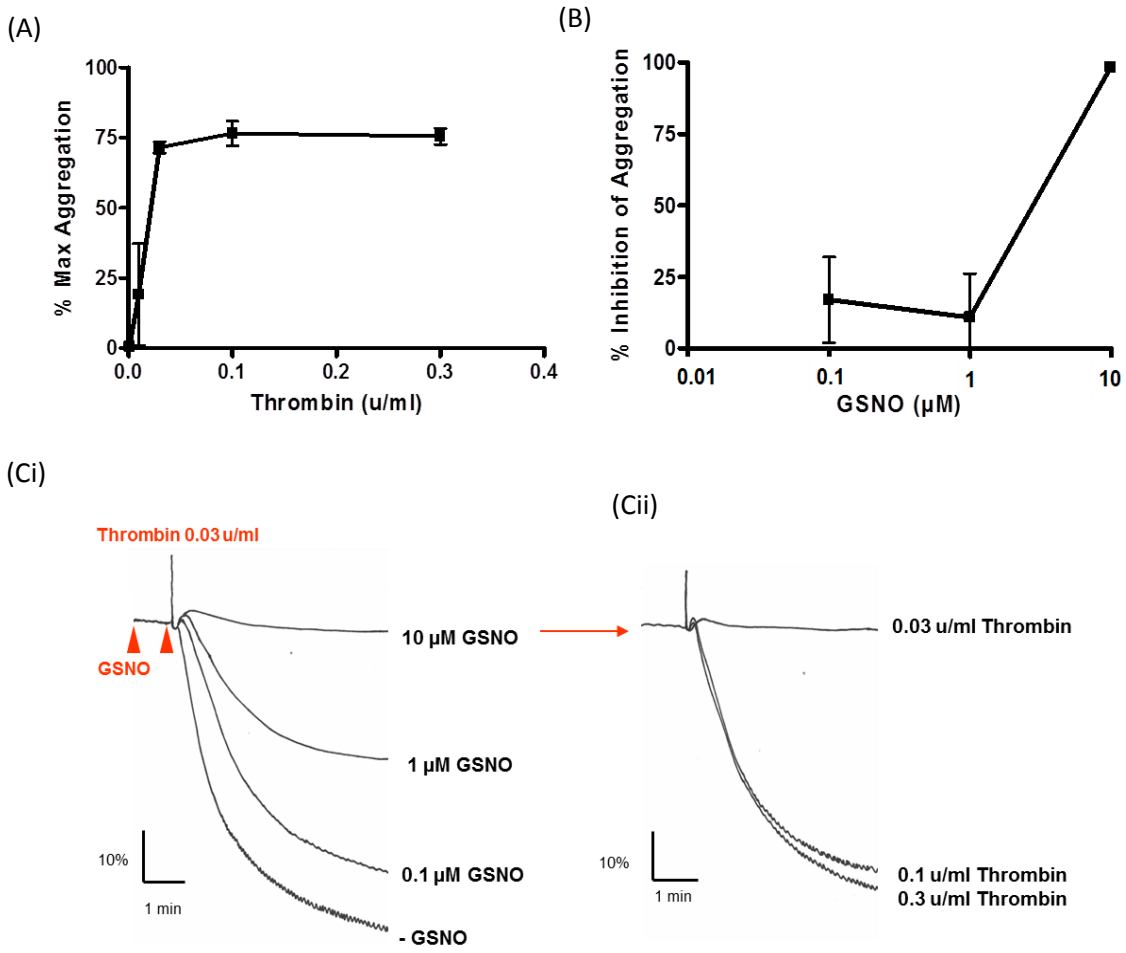

Figure 5. *GSNO mediates concentration dependant inhibition of thrombin stimulated platelet aggregation.* Mean concentration response curves for (A) platelets aggregated with increasing concentrations of thrombin, expressed as percentage of maximal aggregation (n=4), (B) platelets pre-treated with GSNO for 1 min and aggregated sub-maximally with thrombin (0.03 u/ml), expressed as percentage of inhibition of aggregation obtained in the absence of GSNO (n=3). (Ci and Cii) Representative aggregation traces (Ci) GSNO concentration response, (Cii) increasing concentrations of thrombin with a fixed concentration of GSNO (10 µM). Arrow heads indicate addition of NO donor or agonist. Experiments were conducted in aggregometer cuvettes with stirring at 37°C.

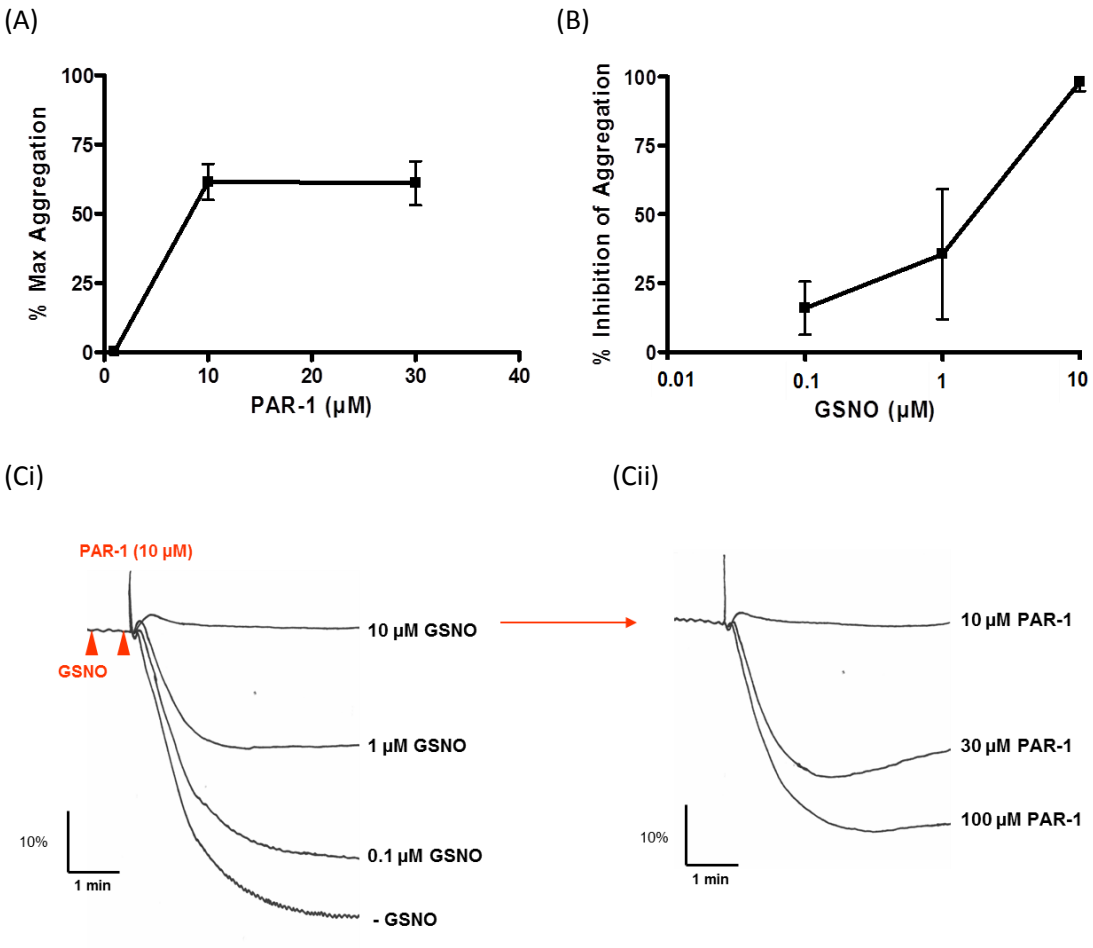

Figure 6. *GSNO mediates concentration dependant inhibition of PAR-1 stimulated platelet aggregation.* Mean concentration response curves for (A) platelets aggregated with increasing concentrations of PAR-1, expressed as percentage of maximal aggregation (n=3), (B) GSNO treated platelets aggregated sub-maximally with PAR-1 (10 µM), expressed as percentage of inhibition of aggregation obtained in the absence of GSNO (n=3). (Ci and Cii) Representative aggregation traces; (Ci) GSNO concentration response, (Cii) increasing concentrations of PAR-1 with a fixed concentration of GSNO (10 µM). Arrow heads indicate addition of NO donor or agonist. Experiments were conducted in aggregometer cuvettes with stirring at 37°C.

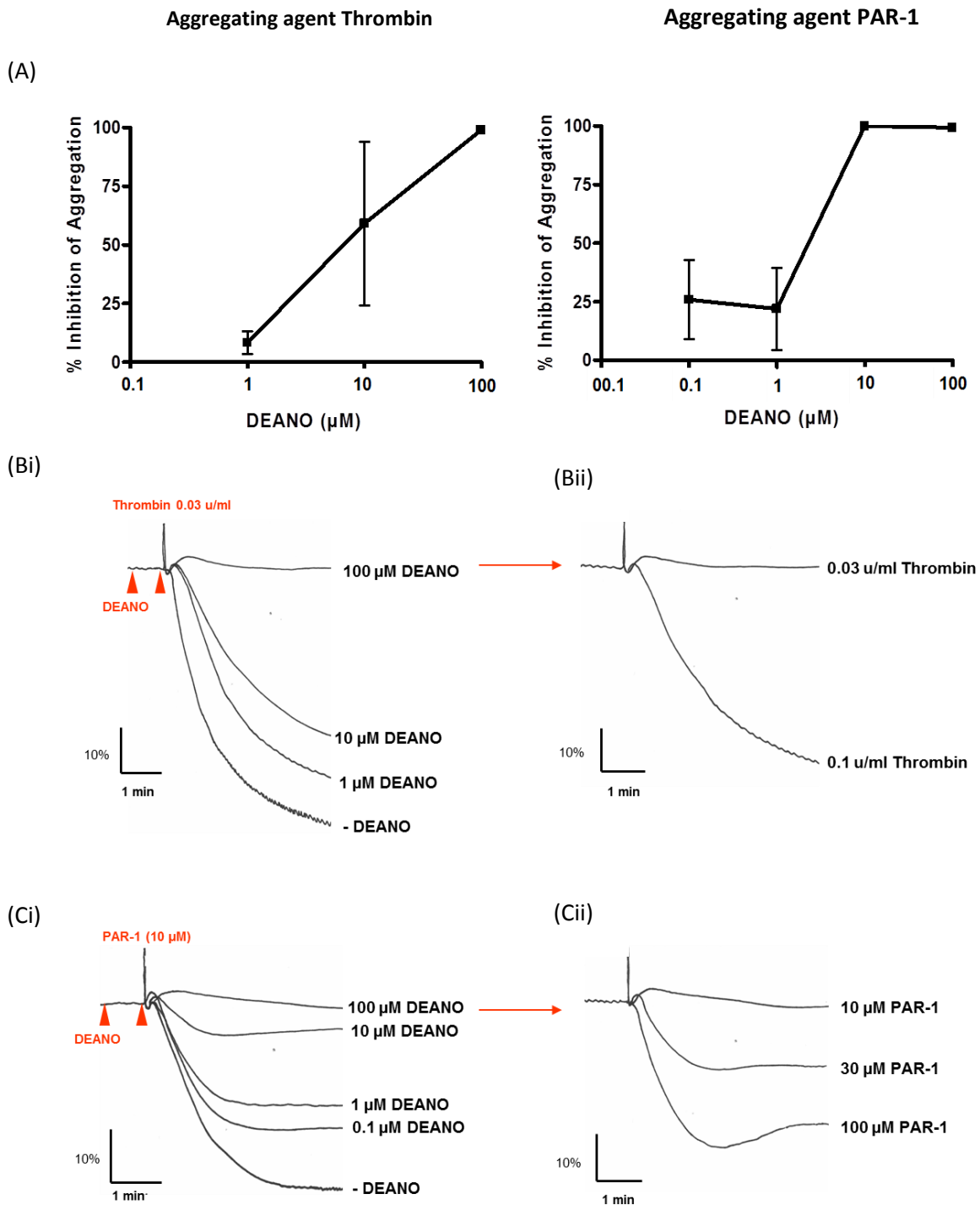
Aggregating agent Thrombin
Aggregating agent PAR-1
(A)
% Inhibition of Aggregation
100
75
50
25
0
0.1
1
10
100
DEANO (µM)
% Inhibition of Aggregation
100
75
50
25
0
00.1
0.1
1
10
100
DEANO (µM)
(Bi)
Thrombin 0.03 u/ml
DEANO
100 µM DEANO
10 µM DEANO
1 µM DEANO
- DEANO
10%
1 min
(Bii)
0.03 u/ml Thrombin
0.1 u/ml Thrombin
10%
1 min
(Ci)
PAR-1 (10 µM)
DEANO
100 µM DEANO
10 µM DEANO
1 µM DEANO
0.1 µM DEANO
- DEANO
10%
1 min
(Cii)
10 µM PAR-1
30 µM PAR-1
100 µM PAR-1
10%
1 min

Figure 7. *DEANO mediates concentration dependant inhibition of thrombin or PAR-1 stimulated platelet aggregation.* (A) Mean concentration response curves to DEANO treated platelets aggregated sub-maximally with thrombin (0.03 u/ml) or PAR-1 (10 µM), expressed as percentage of inhibition of aggregation obtained in the absence of DEANO (n=3). (B and C) Representative aggregation traces; (Bi or Ci) DEANO concentration response with agonists thrombin (0.03 u/ml) or PAR-1 (10 µM), (Bii or Cii) increasing concentrations of thrombin or PAR-1 with a fixed concentration of DEANO (100 µM). Arrow heads indicate addition of NO donor or agonist. Experiments were conducted in aggregometer cuvettes with stirring at 37°C.

.

(A)

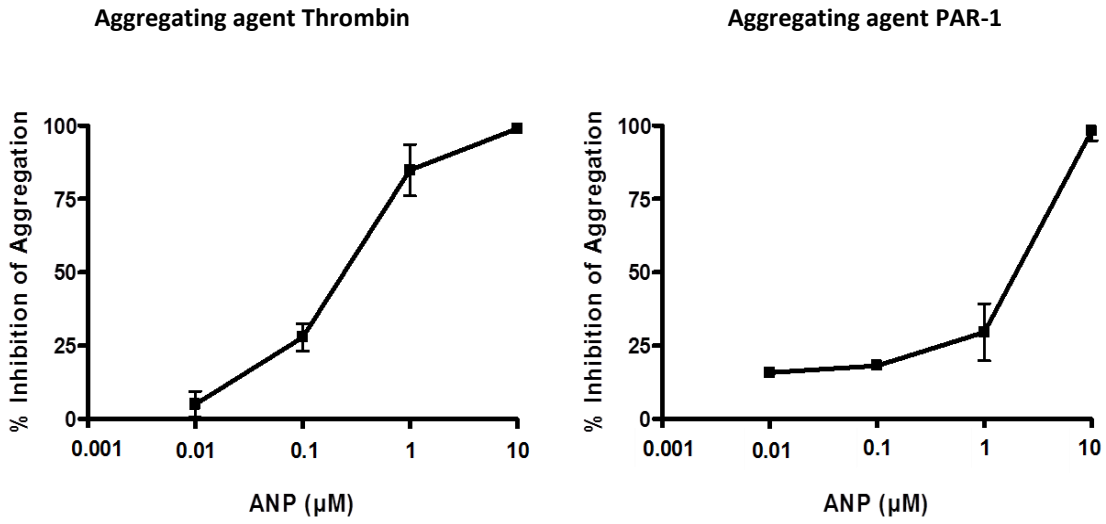

(Bi)

(Bii)

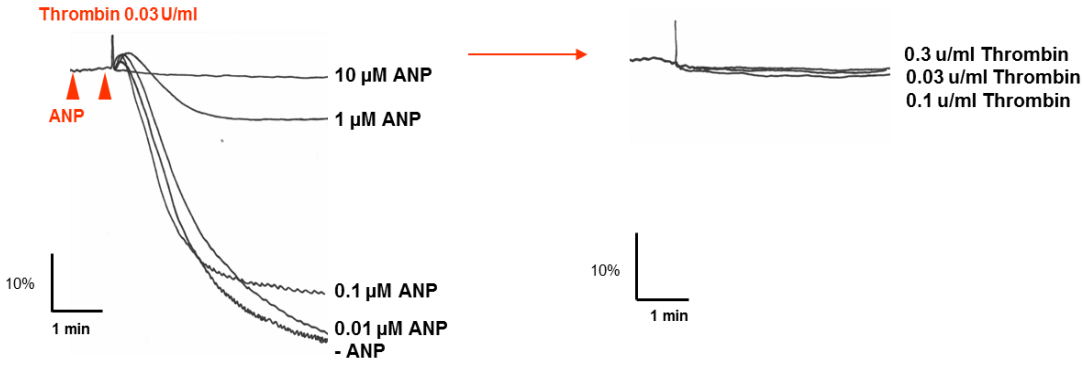

(Ci)

(Cii)

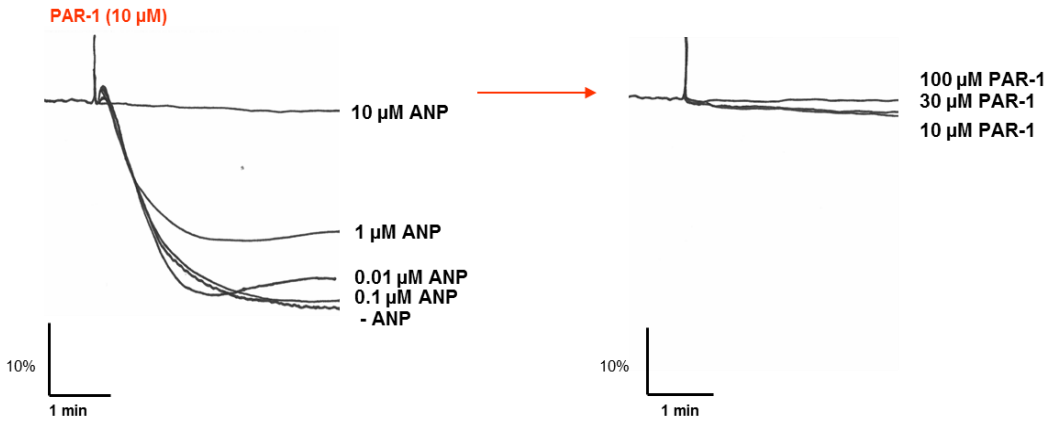

Figure 8. *ANP mediates concentration dependant inhibition of aggregation in thrombin and PAR-1 stimulated platelets.* (A) Mean concentration response curves to ANP treated platelets aggregated sub-maximally with thrombin (0.03 u/ml) or PAR-1 (10 µM), expressed as percentage of inhibition of aggregation obtained in the absence of ANP (n=3 except for points 0.01 µM and 0.1 µM ANP when aggregating with PAR-1; n=1). (B and C) Representative aggregation traces; (Bi or Ci) ANP concentration response with agonists thrombin (0.03 u/ml) or PAR-1 (10 µM), (Bii or Cii) increasing concentration of thrombin or PAR-1 with a fixed concentration of ANP (10 µM). Arrow heads indicate addition of ANP donor or agonist. Experiments were conducted in aggregometer cuvettes with stirring at 37°C.

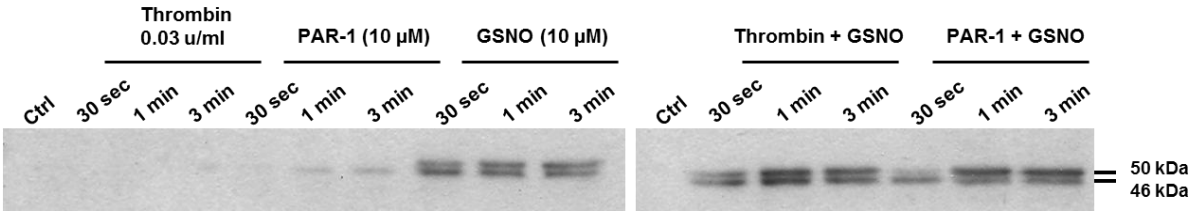

Figure 9. *GSNO mediated VASP phosphorylation in thrombin and PAR-1 stimulated platelets.* Washed platelets (5 x 10^8/ml) were incubated with GSNO or PBS and stimulated with thrombin, PAR-1 or left unstimulated for control or platelets treated with GSNO alone. Samples were lysed with 5 X sample buffer, proteins separated by SDS-PAGE and western blotted for phospho-VASP (Ser239). Molecular weight markers indicated to the right (n=1).

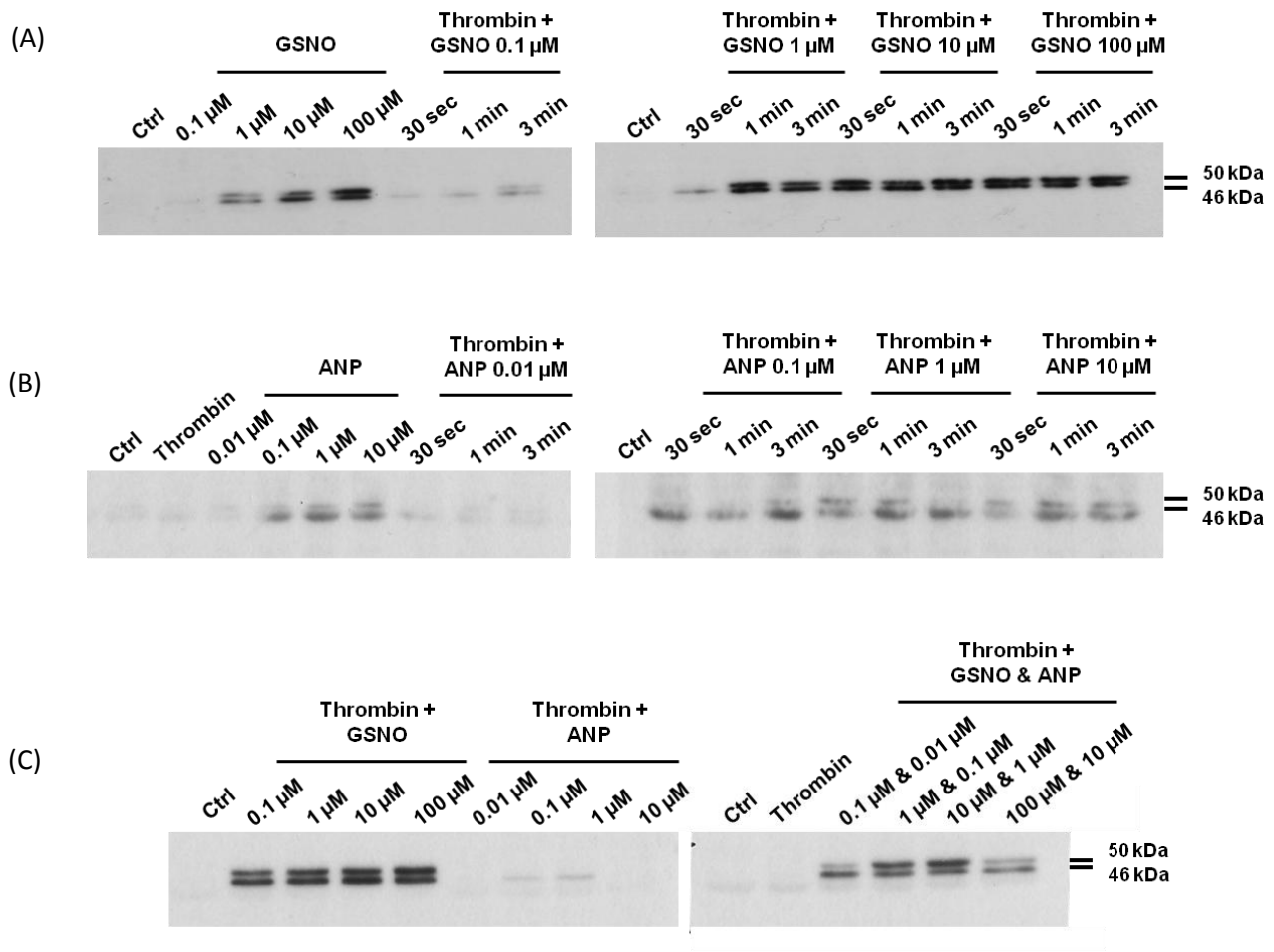

Figure 10. *Concentration and time dependent phosphorylation of VASP (Ser239) by GSNO and ANP.* Washed platelets (5 x 10^8/ml) were incubated with different concentrations of GSNO (A & C), ANP (B & C), ANP and GSNO together (C) or PBS one minute prior to stimulation with thrombin (0.03 u/ml) or left unstimulated for control platelets. Samples were lysed at different time points with 5 X sample buffer, proteins separated by SDS-PAGE and western blotted for phospho-VASP (Ser239). Washed platelets prepared for C are from a different donor to A and B, which are from the same donor. Molecular weight markers indicated to the right. (n=1)

(A)

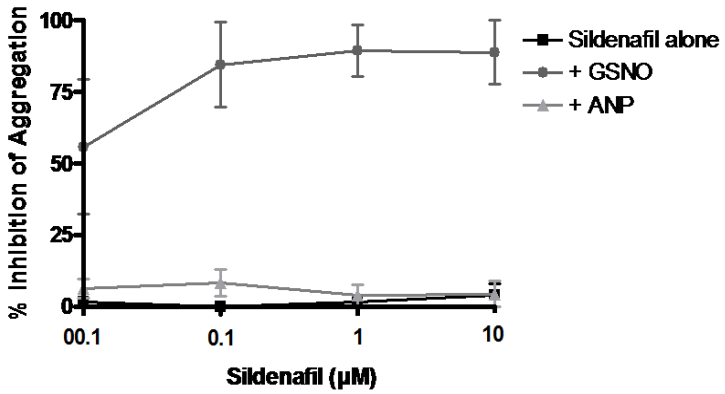
% Inhibition of Aggregation
100
75
50
25
0
00.1
0.1
1
10
Sildenafil (μM)
Sildenafil alone
+ GSNO
+ ANP

(Bi)

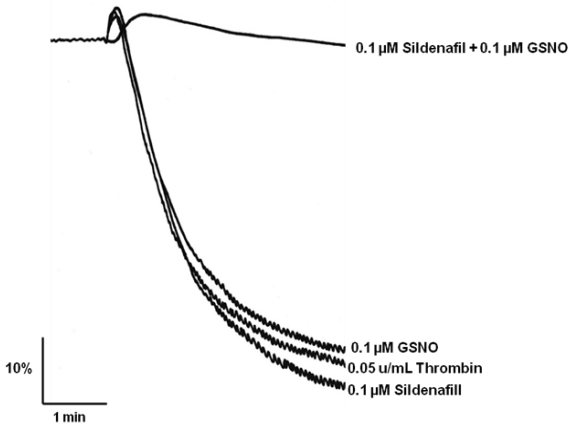
0.1 μM Sildenafil + 0.1 μM GSNO
0.1 μM GSNO
0.05 u/mL Thrombin
0.1 μM Sildenafill
10%
1 min

(Bii)

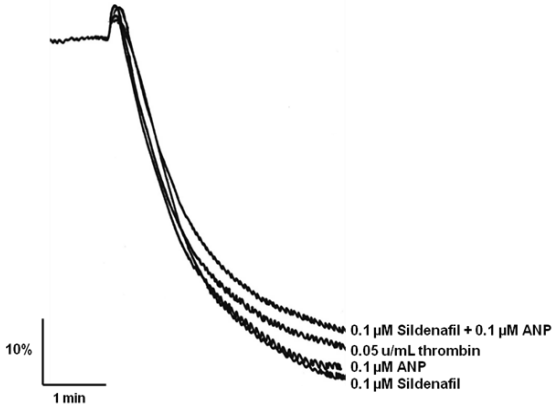
0.1 μM Sildenafil + 0.1 μM ANP
0.05 u/mL thrombin
0.1 μM ANP
0.1 μM Sildenafil
10%
1 min

(C)

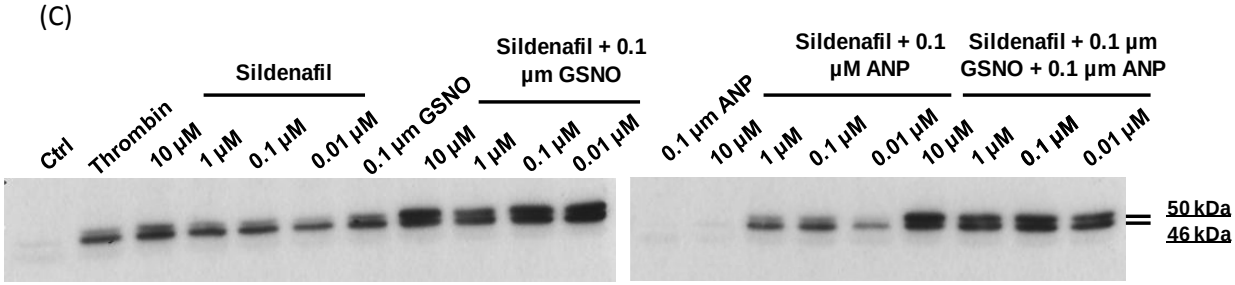
Ctrl
Thrombin
Sildenafil
10 μM
1 μM
0.1 μM
0.01 μM
Sildenafil + 0.1 μm GSNO
0.1 μm GSNO
10 μM
1 μM
0.1 μM
0.01 μM
Sildenafil + 0.1 μM ANP
0.1 μm ANP
10 μM
1 μM
0.1 μM
0.01 μM
Sildenafil + 0.1 μm GSNO + 0.1 μm ANP
10 μM
1 μM
0.1 μM
0.01 μM
50 kDa
46 kDa

Figure 11. *Sildenafil enhances platelet inhibition by GSNO but not ANP* (A) Mean concentration response plots to platelets treated with sildenafil alone or additionally with GSNO (0.1 µM) or ANP (0.1 µM) and aggregated sub-maximally with thrombin (0.05 u/ml) (n=3). (Bi and Bii) Representative aggregation traces for GSNO (Bi) and ANP (Bii) treated platelets. (C) Washed platelets (5 x 10^8/ml) were treated where indicated with sildenafil, GSNO or ANP prior to stimulation with thrombin (0.05 u/ml) or left unstimulated for control platelets. Samples were lysed at 1 min post stimulation with 5 X sample buffer, proteins separated by SDS-PAGE and western blotted for phospho-VASP (Ser239) (n=1). Experiments were conducted in aggregometer cuvettes with stirring at 37°C. Molecular weight markers indicated to the right.

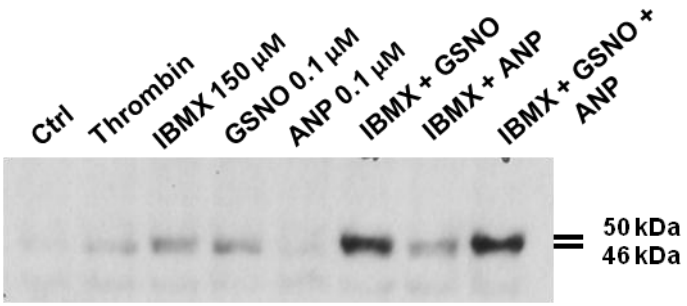

Figure 12. *IBMX enhances VASP phosphorylation in GSNO but not ANP treated platelets.* Washed platelets (5 x 10^8/ml) were treated where indicated with IBMX, GSNO and ANP prior to stimulation with thrombin (0.05 u/ml) or left unstimulated for control platelets. Samples were lysed at 1 min post stimulation with 5 X sample buffer, proteins separated by SDS-PAGE and western blotted for phospho-VASP (Ser239). Experiments were conducted in aggregometer curvettes with stirring at 37°C. Molecular weight markers indicated to the right.

References

1. Hoffbrand, A.V., *Postgraduate haematology*. 6th ed. 2011, Chichester ; Hoboken, NJ: Wiley-Blackwell. xii, 1061 p.
2. Watson, S.P., J.M. Herbert, and A.Y. Pollitt, *GPVI and CLEC-2 in hemostasis and vascular integrity.* J Thromb Haemost, 2010. **8**(7): p. 1456-67.
3. Gibbins, J., et al., *Tyrosine phosphorylation of the Fc receptor gamma-chain in collagen-stimulated platelets.* J Biol Chem, 1996. **271**(30): p. 18095-9.
4. Severin, S., et al., *Syk-dependent phosphorylation of CLEC-2: a novel mechanism of hem-immunoreceptor tyrosine-based activation motif signaling.* J Biol Chem, 2011. **286**(6): p. 4107-16.
5. Watson, S.P., et al., *GPVI and integrin alphaIIb beta3 signaling in platelets.* J Thromb Haemost, 2005. **3**(8): p. 1752-62.
6. Suzuki-Inoue, K., et al., *A novel Syk-dependent mechanism of platelet activation by the C-type lectin receptor CLEC-2.* Blood, 2006. **107**(2): p. 542-9.
7. Suzuki-Inoue, K., et al., *Involvement of the snake toxin receptor CLEC-2, in podoplanin-mediated platelet activation, by cancer cells.* J Biol Chem, 2007. **282**(36): p. 25993-6001.
8. May, F., et al., *CLEC-2 is an essential platelet-activating receptor in hemostasis and thrombosis.* Blood, 2009. **114**(16): p. 3464-72.
9. Suzuki-Inoue, K., et al., *Essential in vivo roles of the C-type lectin receptor CLEC-2: embryonic/neonatal lethality of CLEC-2-deficient mice by blood/lymphatic misconnections and impaired thrombus formation of CLEC-2-deficient platelets.* J Biol Chem, 2010. **285**(32): p. 24494-507.
10. Hughes, C.E., et al., *CLEC-2 is not required for platelet aggregation at arteriolar shear.* J Thromb Haemost, 2010. **8**(10): p. 2328-32.
11. Hughes, C.E., et al., *CLEC-2 activates Syk through dimerization.* Blood, 2010. **115**(14): p. 2947-55.

12. Oliver, G., *Lymphatic vasculature development.* Nat Rev Immunol, 2004. **4**(1): p. 35-45.
13. Sabin, F.R., *On the origin of the lymphatic system from the veins and the development of the lymph hearts and thoracic duct in the pig.* American Journal of Anatomy, 1902. **1**(3): p. 367-389.
14. Srinivasan, R.S., et al., *Lineage tracing demonstrates the venous origin of the mammalian lymphatic vasculature.* Genes Dev, 2007. **21**(19): p. 2422-32.
15. Banerji, S., et al., *LYVE-1, a new homologue of the CD44 glycoprotein, is a lymph-specific receptor for hyaluronan.* J Cell Biol, 1999. **144**(4): p. 789-801.
16. Wigle, J.T., et al., *An essential role for Prox1 in the induction of the lymphatic endothelial cell phenotype.* EMBO J, 2002. **21**(7): p. 1505-13.
17. Tammela, T. and K. Alitalo, *Lymphangiogenesis: Molecular mechanisms and future promise.* Cell, 2010. **140**(4): p. 460-76.
18. Bertozzi, C.C., P.R. Hess, and M.L. Kahn, *Platelets: covert regulators of lymphatic development.* Arterioscler Thromb Vasc Biol, 2010. **30**(12): p. 2368-71.
19. Schacht, V., et al., *T1alpha/podoplanin deficiency disrupts normal lymphatic vasculature formation and causes lymphedema.* EMBO J, 2003. **22**(14): p. 3546-56.
20. Uhrin, P., et al., *Novel function for blood platelets and podoplanin in developmental separation of blood and lymphatic circulation.* Blood, 2010. **115**(19): p. 3997-4005.
21. Turner, M., et al., *Perinatal lethality and blocked B-cell development in mice lacking the tyrosine kinase Syk.* Nature, 1995. **378**(6554): p. 298-302.
22. Clements, J.L., et al., *Fetal hemorrhage and platelet dysfunction in SLP-76-deficient mice.* J Clin Invest, 1999. **103**(1): p. 19-25.
23. Ichise, H., et al., *Phospholipase Cgamma2 is necessary for separation of blood and lymphatic vasculature in mice.* Development, 2009. **136**(2): p. 191-5.
24. Cui, Y.Z., et al., *Optimal protocol for total body irradiation for allogeneic bone marrow transplantation in mice.* Bone Marrow Transplant, 2002. **30**(12): p. 843-9.

25. Goker, H., I.C. Haznedaroglu, and N.J. Chao, *Acute graft-vs-host disease: pathobiology and management.* Exp Hematol, 2001. **29**(3): p. 259-77.
26. Gordon, E.J., N.W. Gale, and N.L. Harvey, *Expression of the hyaluronan receptor LYVE-1 is not restricted to the lymphatic vasculature; LYVE-1 is also expressed on embryonic blood vessels.* Dev Dyn, 2008. **237**(7): p. 1901-9.
27. Helbling, P.M., D.M. Saulnier, and A.W. Brandli, *The receptor tyrosine kinase EphB4 and ephrin-B ligands restrict angiogenic growth of embryonic veins in Xenopus laevis.* Development, 2000. **127**(2): p. 269-78.
28. Mulugeta, S. and M.F. Beers, *Surfactant protein C: its unique properties and emerging immunomodulatory role in the lung.* Microbes Infect, 2006. **8**(8): p. 2317-23.
29. Fox, J.G., *The mouse in biomedical research*. 2nd ed. American College of Laboratory Animal Medicine series. 2007, Amsterdam ; Boston: Elsevier, AP. v. <2-4>.
30. ten Berg, M.J., et al., *Discriminative value of platelet size indices for the identification of the mechanism of chemotherapy-induced thrombocytopenia.* Biomarkers, 2011. **16**(1): p. 51-7.
31. Haanen, C. and I. Vermes, *Apoptosis: programmed cell death in fetal development.* Eur J Obstet Gynecol Reprod Biol, 1996. **64**(1): p. 129-33.
32. Oertel, M., et al., *Cell competition leads to a high level of normal liver reconstitution by transplanted fetal liver stem/progenitor cells.* Gastroenterology, 2006. **130**(2): p. 507-20; quiz 590.
33. Schindowski, K., et al., *Age-related increase of oxidative stress-induced apoptosis in mice prevention by Ginkgo biloba extract (EGb761).* J Neural Transm, 2001. **108**(8-9): p. 969-78.
34. Williams, M.C., et al., *T1 alpha protein is developmentally regulated and expressed by alveolar type I cells, choroid plexus, and ciliary epithelia of adult rats.* Am J Respir Cell Mol Biol, 1996. **14**(6): p. 577-85.
35. Cheng, A.M., et al., *Syk tyrosine kinase required for mouse viability and B-cell development.* Nature, 1995. **378**(6554): p. 303-6.
36. Ramirez, M.I., et al., *T1alpha, a lung type I cell differentiation gene, is required for normal lung cell proliferation and alveolus formation at birth.* Dev Biol, 2003. **256**(1): p. 61-72.

37. Warburton, D., et al., *Lung organogenesis.* Curr Top Dev Biol, 2010. **90**: p. 73-158.
38. Paris, F., et al., *Endothelial apoptosis as the primary lesion initiating intestinal radiation damage in mice.* Science, 2001. **293**(5528): p. 293-7.
39. Abtahian, F., et al., *Regulation of blood and lymphatic vascular separation by signaling proteins SLP-76 and Syk.* Science, 2003. **299**(5604): p. 247-51.
40. Harrington, N.P., et al., *Radiation damage and immune suppression in splenic mononuclear cell populations.* Clin Exp Immunol, 1997. **107**(2): p. 417-24.
41. Ferrara, J.L., R. Levy, and N.J. Chao, *Pathophysiologic mechanisms of acute graft-vs.-host disease.* Biol Blood Marrow Transplant, 1999. **5**(6): p. 347-56.
42. Li, X.M., et al., *Bone marrow sinusoidal endothelial cells undergo nonapoptotic cell death and are replaced by proliferating sinusoidal cells in situ to maintain the vascular niche following lethal irradiation.* Exp Hematol, 2008. **36**(9): p. 1143-1156.
43. Walter, U. and S. Gambaryan, *cGMP and cGMP-dependent protein kinase in platelets and blood cells.* Handb Exp Pharmacol, 2009(191): p. 533-48.
44. Jackson, S.P., *The growing complexity of platelet aggregation.* Blood, 2007. **109**(12): p. 5087-95.
45. Schwarz, U.R., U. Walter, and M. Eigenthaler, *Taming platelets with cyclic nucleotides.* Biochem Pharmacol, 2001. **62**(9): p. 1153-61.
46. Fischmeister, R., et al., *Compartmentation of cyclic nucleotide signaling in the heart: the role of cyclic nucleotide phosphodiesterases.* Circ Res, 2006. **99**(8): p. 816-28.
47. Reffelmann, T. and R.A. Kloner, *Therapeutic potential of phosphodiesterase 5 inhibition for cardiovascular disease.* Circulation, 2003. **108**(2): p. 239-44.
48. Trepakova, E.S., R.A. Cohen, and V.M. Bolotina, *Nitric oxide inhibits capacitative cation influx in human platelets by promoting sarcoplasmic/endoplasmic reticulum Ca2+-ATPase-dependent refilling of Ca2+ stores.* Circ Res, 1999. **84**(2): p. 201-9.

49. Antl, M., et al., *IRAG mediates NO/cGMP-dependent inhibition of platelet aggregation and thrombus formation.* Blood, 2007. **109**(2): p. 552-9.
50. Wang, G.R., et al., *Mechanism of platelet inhibition by nitric oxide: in vivo phosphorylation of thromboxane receptor by cyclic GMP-dependent protein kinase.* Proc Natl Acad Sci U S A, 1998. **95**(9): p. 4888-93.
51. Aszodi, A., et al., *The vasodilator-stimulated phosphoprotein (VASP) is involved in cGMP- and cAMP-mediated inhibition of agonist-induced platelet aggregation, but is dispensable for smooth muscle function.* EMBO J, 1999. **18**(1): p. 37-48.
52. Bear, J.E. and F.B. Gertler, *Ena/VASP: towards resolving a pointed controversy at the barbed end.* J Cell Sci, 2009. **122**(Pt 12): p. 1947-53.
53. Harbeck, B., et al., *Phosphorylation of the vasodilator-stimulated phosphoprotein regulates its interaction with actin.* J Biol Chem, 2000. **275**(40): p. 30817-25.
54. Wentworth, J.K., G. Pula, and A.W. Poole, *Vasodilator-stimulated phosphoprotein (VASP) is phosphorylated on Ser157 by protein kinase C-dependent and -independent mechanisms in thrombin-stimulated human platelets.* Biochem J, 2006. **393**(Pt 2): p. 555-64.
55. Massberg, S., et al., *Enhanced in vivo platelet adhesion in vasodilator-stimulated phosphoprotein (VASP)-deficient mice.* Blood, 2004. **103**(1): p. 136-42.
56. Potter, L.R., S. Abbey-Hosch, and D.M. Dickey, *Natriuretic peptides, their receptors, and cyclic guanosine monophosphate-dependent signaling functions.* Endocr Rev, 2006. **27**(1): p. 47-72.
57. Strom, T.M., J. Weil, and F. Bidlingmaier, *Platelet receptors for atrial natriuretic peptide in man.* Life Sci, 1987. **40**(8): p. 769-73.
58. De Caterina, R., et al., *Effects of atrial natriuretic factor on human platelet function.* Life Sci, 1985. **37**(15): p. 1395-402.
59. Loeb, A.L. and A.R. Gear, *Potentiation of platelet aggregation by atrial natriuretic peptide.* Life Sci, 1988. **43**(9): p. 731-8.
60. Ulker, S., et al., *Platelet aggregation and atrial natriuretic peptide.* Gen Pharmacol, 1995. **26**(6): p. 1409-12.
61. Andreassi, M.G., et al., *Up-regulation of 'clearance' receptors in patients with chronic heart failure: a possible explanation for the resistance to*

biological effects of cardiac natriuretic hormones. Eur J Heart Fail, 2001. **3**(4): p. 407-14.

62. Castro, L.R., et al., *Cyclic guanosine monophosphate compartmentation in rat cardiac myocytes.* Circulation, 2006. **113**(18): p. 2221-8.
63. Wilson, L.S., et al., *Compartmentation and compartment-specific regulation of PDE5 by protein kinase G allows selective cGMP-mediated regulation of platelet functions.* Proc Natl Acad Sci U S A, 2008. **105**(36): p. 13650-5.
64. Zabel, U., et al., *Calcium-dependent membrane association sensitizes soluble guanylyl cyclase to nitric oxide.* Nat Cell Biol, 2002. **4**(4): p. 307-11.
65. Muller, D., et al., *Spatiotemporal regulation of the two atrial natriuretic peptide receptors in testis.* Endocrinology, 2004. **145**(3): p. 1392-401.
66. Homer, K.L. and J.C. Wanstall, *Inhibition of rat platelet aggregation by the diazeniumdiolate nitric oxide donor MAHMA NONOate.* Br J Pharmacol, 2002. **137**(7): p. 1071-81.
67. Bilodeau, M.L. and H.E. Hamm, *Regulation of protease-activated receptor (PAR) 1 and PAR4 signaling in human platelets by compartmentalized cyclic nucleotide actions.* J Pharmacol Exp Ther, 2007. **322**(2): p. 778-88.
68. Zhang, W. and R.W. Colman, *Thrombin regulates intracellular cyclic AMP concentration in human platelets through phosphorylation/activation of phosphodiesterase 3A.* Blood, 2007. **110**(5): p. 1475-82.
69. Piggott, L.A., et al., *Natriuretic peptides and nitric oxide stimulate cGMP synthesis in different cellular compartments.* J Gen Physiol, 2006. **128**(1): p. 3-14.
70. Airhart, N., et al., *Atrial natriuretic peptide induces natriuretic peptide receptor-cGMP-dependent protein kinase interaction.* J Biol Chem, 2003. **278**(40): p. 38693-8.
71. Bryan, P.M. and L.R. Potter, *The atrial natriuretic peptide receptor (NPR-A/GC-A) is dephosphorylated by distinct microcystin-sensitive and magnesium-dependent protein phosphatases.* J Biol Chem, 2002. **277**(18): p. 16041-7.
72. Hou, Y., et al., *Activation of cGMP-dependent protein kinase by protein kinase C.* J Biol Chem, 2003. **278**(19): p. 16706-12.

73. Gudmundsdottir, I.J., et al., *Sildenafil potentiates nitric oxide mediated inhibition of human platelet aggregation.* Biochem Biophys Res Commun, 2005. **337**(1): p. 382-5.
74. Maurice, D.H. and R.J. Haslam, *Nitroprusside enhances isoprenaline-induced increases in cAMP in rat aortic smooth muscle.* Eur J Pharmacol, 1990. **191**(3): p. 471-5.
75. Dunkern, T.R. and A. Hatzelmann, *The effect of Sildenafil on human platelet secretory function is controlled by a complex interplay between phosphodiesterases 2, 3 and 5.* Cell Signal, 2005. **17**(3): p. 331-9.
76. Baliga, R.S., et al., *Synergy between natriuretic peptides and phosphodiesterase 5 inhibitors ameliorates pulmonary arterial hypertension.* Am J Respir Crit Care Med, 2008. **178**(8): p. 861-9.
77. Castro, L.R., J. Schittl, and R. Fischmeister, *Feedback control through cGMP-dependent protein kinase contributes to differential regulation and compartmentation of cGMP in rat cardiac myocytes.* Circ Res, 2010. **107**(10): p. 1232-40.
78. Anand-Srivastava, M.B., M.R. Sairam, and M. Cantin, *Ring-deleted analogs of atrial natriuretic factor inhibit adenylate cyclase/cAMP system. Possible coupling of clearance atrial natriuretic factor receptors to adenylate cyclase/cAMP signal transduction system.* J Biol Chem, 1990. **265**(15): p. 8566-72.
79. Chen, H., et al., *Atrial natriuretic peptide-initiated cGMP pathways regulate vasodilator-stimulated phosphoprotein phosphorylation and angiogenesis in vascular endothelium.* J Biol Chem, 2008. **283**(7): p. 4439-47.
80. Gambaryan, S., et al., *Potent inhibition of human platelets by cGMP analogs independent of cGMP-dependent protein kinase.* Blood, 2004. **103**(7): p. 2593-600.